LUND
UNIVERSITY

Study of Dark Matter Models in Astrophysics and Particle Physics

Isabelle John

Thesis submitted for the degree of Master of Science
Project Duration: January 2018 – May 2019, 60 ECTS
Supervised by Caterina Doglioni (Lund University) and Antonio Boveia (Ohio State University)

Department of Physics
Division of Particle Physics
May 2019

Abstract

From astrophysical and cosmological observations, it is known that most of the matter in the Universe is dark. This matter could be explainable by new particles, not included in the Standard Model of Particle Physics. This work assumes that there exists an interaction between dark matter and Standard Model particles, and investigates if the present relic density of dark matter in the Universe could be satisfied by a model with a vector mediator Z' for a variety of mediator and dark matter masses, as well as coupling constants to dark matter and Standard Model fermions, distinguishing between quark and lepton couplings. The relic density is computed in the standard thermal freeze-out scenario using MadDM, and in the freeze-in scenario using micrOMEGAs. The freeze-out scenario assumes that all dark matter is produced in the early Universe, and then partially annihilates, i.e. "freezes out", to the current amount. In the freeze-in scenario, it is assumed there that is no dark matter in the early Universe and it is produced over time from Standard Model particle annihilations. In this work, it is also shown how the reheating temperature affects the freeze-in relic density. These couplings and masses tested here are chosen so that they could be produced at the LHC. While the relic density can be satisfied by these models in the freeze-out scenario, the freeze-in mechanism requires a very low reheating temperature in order to obtain couplings that the LHC is sensitive to.

In a second part, this work turns to the comparison of dark matter exclusion limits from LHC searches and results from direct detection experiments, concentrating on the latter. Direct detection experiments can detect these relic dark matter particles, and therefore their event rate depends on the local dark matter density and the velocity distribution. These are both uncertain parameters. Using uncertainty calculation methods from different analyses that choose assumptions alternative to the common assumptions made in the Standard Halo Model, deviations of the direct detection experiment exclusion limits are investigated and discussed.

Abbreviations and acronyms

BBN	Big Bang nucleosynthesis
BSM	beyond the Standard Model
CERN	European Organization for Nuclear Research
CL	confidence level
CMB	cosmic microwave background
DM	dark matter
FIMP	frozen-in massive particle, feebly-interacting massive particle
ΛCDM	Lambda cold dark matter
LHC	Large Hadron Collider
MACHO	massive compact halo object
MET	missing transverse energy
MOND	modified Newtonian dynamics
NFW	Navarro-Frenk-White (profile)
PMT	photomultiplier tube
QCD	quantum chromodynamics
QED	quantum electrodynamics
SHM	Standard Halo Model
SM	Standard Model
SUSY	supersymmetry
TLA	trigger-level analysis
TPC	time-projection chamber
WIMP	weakly interacting massive particle

My work and acknowledgments

In chapter 3, the data to make the plots was obtained from MadDM and micrOMEGAs. The code to make the plots was written by me using ROOT.

For this chapter, I received help and supervision from the micrOMEGAs team, especially A. Goudelis, B. Zaldivar, A. Pukhov and G. Belanger.

In chapter 5, the uncertainty bands from the analysis groups in [1, 2, 3, 4] were added to the summary plot by me. To do so, I modified the code to make the summary plots written by Emma Tolley [5]. The band in 4.3.4 was obtained from code written by me with instructions from the analysis group in [4].

For this chapter, I received inputs, help and supervision from the various teams in the analyses of the uncertainties for direct detection results, especially A. Rappelt, N. Bozorgnia, M. Benito, F. Iocco and A. Cuoco.

I want to thank everyone for their help and collaboration.

My thanks also go to my supervisors, Caterina Doglioni and Antonio Boveia, for their help and everything they have taught me. I appreciate it very much.

Presentation of this work

Results of this work were presented at the following meetings and conferences:

- talk at LHC Dark Matter Working Group meeting, June 2018: *Calculating the relic density for a light vector mediator with MadDM and micrOMEGAs*
- poster at TeVPA Berlin, August 2018: *Calculating the dark matter relic density for a light mediator in freeze-out and freeze-in scenarios with MadDM and micrOMEGAs*
- talk at Partikeldagarna Lund, October 2018: *Freeze-out and freeze-in relic density for a light vector mediator*
- talk at Common Dark Matter subgroup meeting, March 2019: *Summarising uncertainties on dark matter direct detection limits*

Contents

Chapter 1

Introduction

Astrophysical observations suggest the existence of dark matter, but its nature is still unknown [6]. There is evidence that a large amount of the matter in the Universe is not visible: Figure 1.1 illustrates that out of the total energy content of the Universe, only about 5% is made up of ordinary matter, about 27% is dark matter, and the remaining 68% is accounted for by dark energy[1]. This shows how little is understood about the world, and many efforts are made toward unveiling the physics of the Universe. While astrophysics provides evidence of this dark matter in galaxy halos or by analysing the large-scale structure of the Universe, particle physics is searching for new particles that can explain the nature of dark matter.

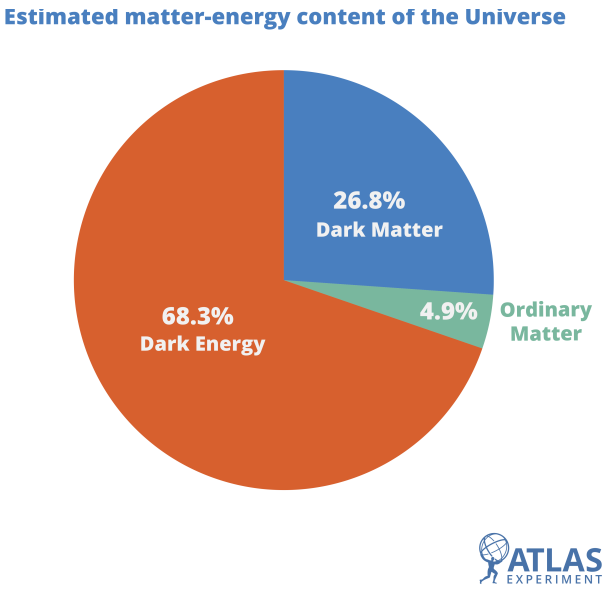

Figure 1.1: Diagram visualising the energy content of the Universe. Figure taken from [8].

This thesis focuses on how observations from astrophysics can be used to set constraints on the particle models of dark matter. It is divided into the following parts: In this first chapter, a background and overview of dark matter models in astrophysics and particle physics is given. In the first part of this work, the dark matter relic density for a vector mediator, a new particle that mediates the interactions of dark matter particles with Standard Model particles, is investigated assuming a variety of masses and couplings to dark matter and Standard Model particles. The tools and models used are described in chapter 2, while the results are presented and discussed in chapter 3. The second part of this work looks at exclusion limits on dark matter models at collider and direct detection experiments, and how the results of the latter can change when making different assumptions about the dark matter density and velocity at the position of the solar system. Direct detection experiments and the methods of this part are explained in chapter 4. The results are presented in chapter 5. Lastly, conclusions and an outlook can be found in chapters 6 and 7.

[1] Not much is known about dark energy, except that it causes the expansion of the Universe to be accelerated [7].

1.1 Astrophysical observations of dark matter

Hints for non-luminous matter components come from astronomical observations. Earliest evidence was found in the 1930s when attempting to determine the mass of the Coma cluster, a large group of galaxies. This was done by measuring its matter content based on the luminous material to approximate the total mass of the cluster, and by measuring its rotation curve assuming the cluster to rotate like a solid. The two methods did not give similar results; instead it was concluded that there was more matter in the cluster than what was visible. This non-radiating matter was hence called "dark matter" [9].

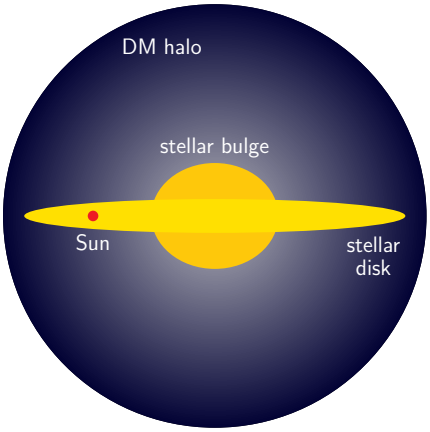

Figure 1.2: This sketch shows the main components of a galaxy, such as the Milky Way. Surrounded by a halo that contains most of the dark matter, the luminous parts of a galaxy are a central stellar bulge and a stellar disk in the plane, that contains stars as well as gas (interstellar medium).

This missing-mass phenomenon occurred again in the 1970s when determining the rotation curves of galaxies [6, 9]. A sketch of a galaxy is shown in figure 1.2. Most of the luminous matter is concentrated in the central stellar bulge which is surrounded by a large disk of stars and gas. Based on the visible matter, one would expect rotational velocities decreasing with further distance from the centre, as stated by

$$F = \frac{GMm}{r^2} = \frac{mv^2}{r} = F_{\text{rad}},$$

where G is Newton's gravitational constant [9]. For a galaxy with mass M where $M(< r)$ is the mass contained inside an orbit at a distance r from the galactic centre, a star with mass m experiences a gravitational force F, orbiting the galactic centre at a rotational velocity v. Since $v = \sqrt{GM(< r)/r}$, the velocity of the star is expected to decrease with $r^{-1/2}$ [9, 10].

Observations show that the rotational velocities instead stay about constant for increasing radius, implying that there must be more matter in the outer regions of the galaxies than is visible. This suggests that galaxies possess halos where most of the galactic dark matter is concentrated (see figure 1.2) [9].

Another source of evidence for dark matter comes from gravitational lensing. From General Relativity it is known that the gravitational potential caused by the mass of an object bends space, and photons travelling past a massive object are deflected by its gravitational potential, similarly how light is deflected when sent through a lens. The

more massive the object is, the stronger is the deflection. This is used for probing dark matter through the discrepancy between the expected gravitation from luminous matter and the actual gravitational potential [6].

Another indication for dark matter comes from the large-scale structure of the Universe. From simulations, it is noticeable that the gravity that forms the large-scale structure observed today has to be more than the visible matter can provide [9].

Dark matter was discovered by astrophysical observations, but one hypothesis suggests that dark matter has a particle explanation. Since, so far, all matter can be described in terms of fundamental particles, particle physics models have also emerged to explain the nature of this dark matter.

1.2 The Standard Model of particle physics

The Standard Model (SM) of particle physics is a quantum field theory, describing the fundamental building blocks of matter and interactions as point-like particles [11], as far as current understanding goes. An overview of the particles in the Standard Model is given in figure 1.3.

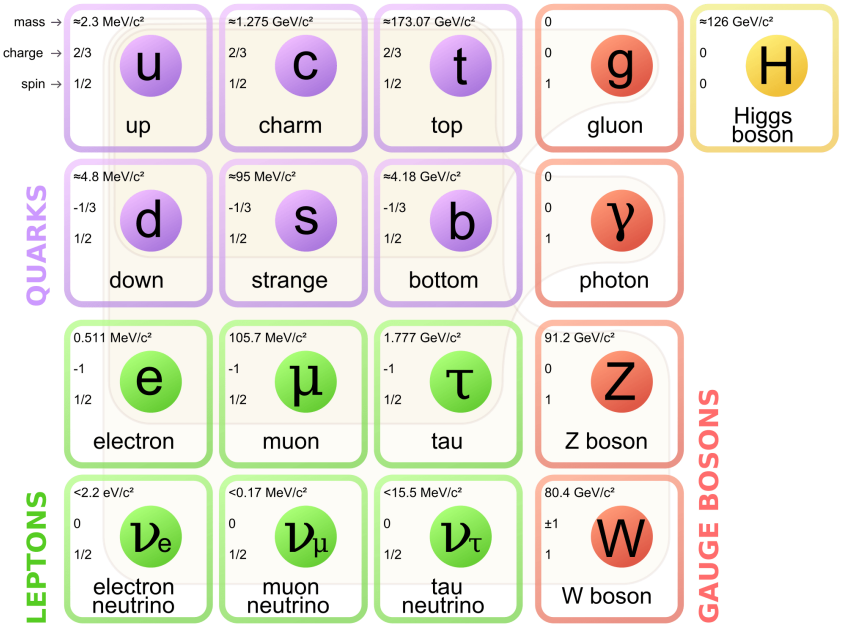

Figure 1.3: The Standard Model of Elementary Particles. Figure taken from [12].

Particles that make up matter are fermions whose spin value is 1/2. There are two groups of fundamental fermions: quarks and leptons, of which exist six particles each, divided into three generations. The quarks are called up (u) and down (d), charm (c) and strange (s), and top (t) and bottom (b). Each carries a fraction of the electric charge (in terms of the elementary charge $e = 1.6 \cdot 10^{-19}$ C, [10]) and a colour charge. There are three charged leptons; the electron e, the muon μ and the tauon τ with -1 electric charge. There are three neutrally charged leptons: the electron neutrino ν_e, the muon neutrino ν_μ and the tau neutrino ν_τ.

Particles in the second and third generation have larger masses compared to the first generation, and are thus unstable and decay into particles of the first generation, i.e. only the first generation particles can form stable structures, meaning that almost all the

matter in the Universe is built from u and d quarks and electrons, as the combinations uud and udd give protons and neutrons, respectively, that, together with electrons, make up atoms.

For each fermion (except possibly for the neutrinos [10]) there exists an antiparticle that is identical in all properties to the particle, except that it has opposite charge [10, 11].

Besides fermions, there are also bosons in the Standard Model, particles with integer spin. The gauge bosons have spin-1 (vector bosons) and propagate the interactions between particles. They are: the gluons g, the photon γ, and the Z^0, W^+ and W^- bosons.

The gluons propagate the strong interaction, described by quantumchromodynamics (QCD). They each carry a combination of a colour and an anticolour charge. The gluons are massless, but their interaction is short ranged due to colour confinement, meaning that particles combine into a colourless state (hadrons). Out of all fermions, only the quarks have a colour charge and can partake in strong interactions. There are three different colour charges, called red (r), green (g) and blue (b), and only a combination of all three colours (baryons) or a colour and an anticolour (mesons) results in a neutral colour charge. In high-energetic particle collisions, quarks and gluons (combined called partons) can be produced or kicked out of their colour-neutral bound state. Due to colour confinement, they cannot exist freely, and quickly fragment into less energetic particles with neutral colour charge. This creates a collimated beam of particles, called a jet. In a detector, each jet indicates the fragmentation of a parton.

The photon is the propagator of the electromagnetic interaction. It is massless and long-ranged. All particles with an electric charge, i.e. the quarks and charged leptons, can undergo electromagnetic interactions. The process of electromagnetism is described by quantumelectrodynamics (QED).

The Z^0 and $W^\pm$ bosons propagate the weak interaction. The Z^0 boson has a mass of about 91 GeV and the $W^\pm$ bosons of 80 GeV [13]. The Z^0 boson is neutrally charged, whereas the two W bosons have electric charge $+1$ and -1. Due to their relatively large mass, the interaction is weak and short-ranged. All fermions can partake in weak interactions [10].

Another boson in the Standard Model is the Higgs boson. It is a scalar boson with spin 0 and no charge, and a mass of 125 GeV [13]. Through the Higgs mechanism, it is responsible for the masses of the Standard Model particles (except possibly for the neutrino masses) [10].

1.2.1 Beyond the Standard Model

While the Standard Model describes well the particle interactions, it cannot account for some observed phenomena. There are many hints that the Standard Model is incomplete. New physics beyond the Standard Model (BSM) is required, and many theoretical extensions to the Standard Model exist. In some of these theories, there exist massive, stable particles which are candidates for particle dark matter, leading to the particle physics interpretation of the astrophysical dark matter phenomenon.

Besides dark matter and dark energy, examples for observations that are not explained in the Standard Model are:

- Gravity: Being one of the four fundamental interactions besides the weak, strong and electromagnetic interaction, gravity has not been explained yet in particle physics terms [10].

- Neutrino masses: Since there are no known right-handed neutrinos (see e.g. [10]), the Higgs mechanism that gives mass to the particles does not work for neutrinos. However, from neutrino oscillations it is known that they have a small mass. Currently, the Standard Model cannot explain this [10].

- Matter-antimatter asymmetry: There is much more matter than antimatter in the Universe, meaning that more particles are produced than antiparticles. A source for this asymmetry has been found in CP (charge-parity) violation in weak decays. However, so far it seems that weak CP violation is not enough to account for the large discrepancy, and there must be another source for the matter-antimatter asymmetry beyond the Standard Model [11].

One of these extensions of the Standard Model is supersymmetry (SUSY). Each fermion (spin-half particle) has a super-partner with integer-spin, and each boson (integer-spin particle) has a spin-half super-partner [10]. Some of these massive particles could be stable and therefore be candidates for dark matter. This means that dark matter could be part of a more general theory such as SUSY. SUSY dark matter candidates are for example the neutralino, possibly the lightest SUSY particle, and the very weakly-interacting gravitino [14].

1.3 ΛCDM cosmology and dark matter properties

Current evidence indicates that the Universe emerged about 13.7 billion years ago, in an event called the Big Bang [9]. The Universe was extremely dense and hot. Some theories suggest that shortly after its creation, there was a phase of very rapid expansion called inflation. After this, the Universe was still very dense and hot, so matter existed in a quark-gluon plasma, and matter and radiation were in thermal equilibrium. When the Universe cooled sufficiently, protons could form from quarks. As the energy of the photons was in the order of the binding energy between nucleons (protons and neutrons), nuclei could only form when the Universe cooled more, and the nucleosynthesis of light elements and isotopes started. This is called Big Bang nucleosynthesis (BBN). This was the time – when the age of the Universe was about 1 s [9] – when most of the matter was created, and the matter observable today is a relic from that epoch. The current amount of dark matter in the Universe is referred to as the relic density of dark matter. More details on this can be found in section 2.1.2.

Atoms formed about 380 000 years after the Big Bang, when the Universe was cool enough ($T = 3000$ K ≈ 1 eV) for protons and electrons to bind without constantly being ionised by photons [9, 15]. This is called recombination, and the Universe became transparent for photons so that they could decouple from the matter and travel unhindered without being absorbed (i.e. their mean free path is equal to the age of the Universe [9]). These first emitted photons in the Universe are measurable as a microwave signal coming from every direction. It is called the cosmic microwave background (CMB). As these photons have been travelling since almost the beginning of the Universe, their short wavelength has been extremely redshifted ($z = 1100$)[2], turning them into radiation with microwave wavelength, corresponding to a temperature of about 2.73 K [7, 9].

[2]The redshift, given by $z = \frac{\lambda_{\text{obs}} - \lambda_{\text{em}}}{\lambda_{\text{em}}}$, is obtained from the relation between the emitted wavelength of an object, λ_{em} and the wavelength observed on Earth, λ_{obs}. The shift can be determined by looking at the shift of the emission lines in the electromagnetic spectrum of the object [9].

The CMB possesses anisotropies, which are small fluctuations in the temperature spectrum in the order of $\Delta T/T = 10^{-5}$. The large-scale structure of the Universe observable today displays galaxy clusters arranged in filament structures, with large voids in between. This results from temperature fluctuations in the early Universe as indicated by the CMB anisotropies [9]. Measurements of the CMB provide information about the contents of the Universe. The Universe consists of radiation, matter and vacuum. The total energy density Ω is the sum of all constituents of the Universe,

$$\Omega = \Omega_{\text{rad}} + \Omega_{\text{m}} + \Omega_{\Lambda}, \tag{1.1}$$

where Ω_{rad}, Ω_{m} and Ω_{Λ} are the energy density of radiation, matter and vacuum (dark energy), respectively [9]. Current measurements suggest that $\Omega_{\Lambda} \approx 0.68$ and $\Omega_m \approx 0.32$ where the matter content is divided into the baryonic density $\Omega_{\text{baryon}} \approx 0.05$ and the dark matter density $\Omega_c \approx 0.27$ (c stands for "cold" dark matter, which refers to the non-relativistic velocities of the dark matter particles). This means that 83% of the total matter in the Universe is dark matter, and the visible, ordinary matter makes up only 17% [7].

Often, the densities are given in terms of h^2, a quantity that is related to the Hubble parameter H_0 which is a measure for the expansion rate of the Universe, given by the quotient of an object's velocity v and its distance d to Earth, i.e. $H_0 = v/d$. The Hubble constant relates to h as $h = H_0/\left(100 \text{ km}/(\text{s Mpc})\right)$. Current estimates give $h = 0.67$ [7]. As the dark matter density is $\Omega_c = 0.27$, this becomes $\Omega_c h^2 = 0.12$ [7, 16]. This way, the densities are given independently of the expansion rate and its uncertainties.

Research in astrophysics and cosmology has led to some constraints on the properties of dark matter, creating the ΛCDM model, where Λ stands for the vacuum energy (dark energy) and CDM for cold dark matter. To explain the astrophysical observations, such as the large-scale structure of the Universe, most of the dark matter must be cold [17]. However, a part of the dark matter could be warm (velocities not quite relativistic) and hot (relativistic velocities).

As dark matter in galaxies is predominantly concentrated in the halo surrounding the galaxy (see figure 1.2), dark matter must be dissipationless, meaning that it is unable to cool down and collapse into a disk structure like baryonic matter [9]. However, there could be a small amount of dark matter that is dissipative through some additional "dark radiation", leaving the possibility of a "dark disk" [18].

Most of the dark matter should be collisionless. Evidence for this was found in colliding clusters of galaxies, the so called "Bullet cluster", as well as MACS J0025.4-1222 [6]. Gravitational lensing is used to obtain the mass distribution of the clusters, and the expected mass from baryonic observations is determined. The result shows a spatial discrepancy between the position of the baryonic mass and the bulk of the mass that is accounted for by dark matter. This separation of dark matter and baryonic matter is caused by the collision and merger of two galaxy clusters, indicating that dark matter is collisionless as opposed to the baryonic matter. Due to the collisions the baryonic matter is left behind, while the dark matter parts of the two clusters pass through each other almost unhindered [6, 19]. However, observations from other clusters indicate that dark matter could also be self-interacting [6].

1.4 Dark matter candidates

While this work focuses on the particle explanation of dark matter, there are other explanations for what dark matter could be. It is also possible that dark matter is accounted for by a combination of several of these.

MACHOs

Massive Compact Halo Objects (MACHOs) are non-luminous or faint astronomical objects mostly present in the galaxy halo, with a luminosity too low to be currently detected by telescopes. They can be baryonic or non-baryonic [9]. This could for example be primordial black holes, i.e. black holes that formed early on in the Universe. Remnants of these black holes could account for some of the dark matter [9]. Other options are brown dwarves which are expected to be abundant in galaxies. They are hydrogen-rich objects, star-like, but with a mass too low to start hydrogen fusion, thus remaining faint or non-luminous [20]. However, the non-observation of MACHOs and further constraints suggest that they cannot account for the main component of dark matter [21].

Modified gravity

So far, gravity is still not understood on a particle physics scale. The phenomenology of dark matter implies attractive gravitational properties, and since so far no evidence has been found that dark matter interacts with visible matter in any way besides gravity, an explanation for the observations could be that it is gravity itself that is insufficiently understood, and the description of gravitational attraction between massive objects is only an approximation that breaks down on galactic scales. This is described by theories extending Newton's laws of gravity, called MOND (Modified Newtonian Dynamics) or the relativistic extension TeVeS (tensor-vector-scalar) [6]. However, alternative gravity models are not able to explain all observations thought to originate from dark matter [22].

1.4.1 Particle dark matter

As the Standard Model shows that so far all matter and interactions (besides gravity) can be modelled with elementary particles, one can expect that dark matter is also composed of elementary particles. As mentioned in section 1.2, there are many indications that the Standard Model of particle physics is not complete, and that there exist particles that have not been discovered yet. Many theories beyond the Standard Model require new elementary particles, some of which possess the properties needed to be a dark matter candidate, and dark matter could be part of a more general theory [22].

The dark matter particle candidate has to be sufficiently long-lived, i.e. at least as long as the age of the Universe, to account for the large amount of observable dark matter. It is also possible that there is not just one type of new particle that accounts for dark matter, but instead dark matter particles could arise from several models and together make up dark matter.

Examples for particle dark matter candidates are sterile neutrinos [17, 22], and axions [6, 10, 22]. The candidates relevant for this thesis are weakly-interacting massive particles, called WIMPs, explained in the following section.

WIMPs

WIMPs are a particle candidate for cold dark matter that is simple yet motivated because if WIMPs are in chemical equilibrium in the early Universe, WIMP models are able to reproduce the dark matter relic density observed today [6]. More details on the relic density can be found in section 2.1.2. The WIMP mass can be between about 1 TeV and down to a few GeV and lower [23]. WIMPs interact with Standard Model particles through the weak interaction or a new type of interaction with an interaction strength similar to or smaller than the weak interaction, which is a reason for why they have not been observed yet [13]. They are stable and neutral [22]. WIMPs can for example be stable, massive SUSY particles.

1.5 Interactions between dark matter and Standard Model particles

One way to measure and directly observe dark matter particles is through their interaction with ordinary particles – assuming there exists an interaction between dark matter and Standard Model particles. Based on these interactions, different search strategies for dark matter signals are developed. Figure 1.4 shows the three possible types of interactions of (weakly-interacting) dark matter particles with Standard Model particles. (a) and (b) represent dark matter detection experiments aiming at exclusively detecting and identifying dark matter as such from galactic sources. At collider experiments, shown in (c) and (d), the aim is to produce new kinds of (invisible) particles, some of which can also be dark matter candidates. The different searches are complementary and all types of searches are needed to find dark matter and identify the properties and interactions of the particles.

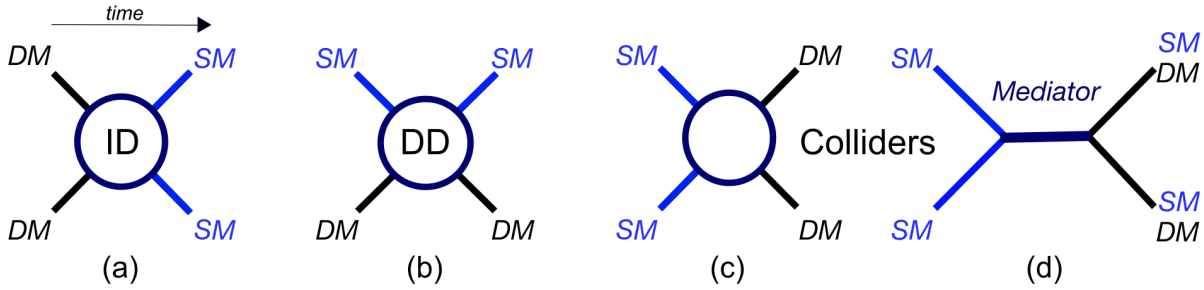

Figure 1.4: Different interactions of dark matter with ordinary matter. (a) direct detection, (b) indirect detection, (c) and (d) collider production/searches. A circle indicates that the nature of the interaction is not known. Figure taken from [24].

1.5.1 Indirect detection experiments

Searches for unexpected signals coming from astrophysical objects are based on the indirect detection (ID) of dark matter, shown in figure 1.4 (a), where two dark matter particles annihilate into two Standard Model particles.

Dark matter annihilation could produce signals like $\chi\bar{\chi} \rightarrow \gamma\gamma, q\bar{q}, W^+W^-$, and some of these can decay further. Detectable signals could thus be e^-e^+, neutrinos or γ rays [22].

A number of telescopes search for these signals. MAGIC [25] and HESS [26] look for TeV γ rays in regions with a large amount of dark matter. Neutrino detectors such as IceCube [27] and SuperKamiokande [28] can search for neutrinos produced by dark matter annihilation, for example in the solar neutrino flux. PAMELA [29] is a satellite that can detect charged particles (e.g. e^-e^+ and $p\bar{p}$). Such signals could also arise from astrophysical objects, such as pulsars, a type of star. So far, no compelling evidence for dark matter annihilation has been found in indirect detection searches [22].

1.5.2 Direct detection experiments

In figure 1.4 (b), the principle of direct detection (DD) experiments is shown. Here, a dark matter particle (possibly WIMP) elastically scatters off a Standard Model particle. The recoil of the Standard Model particle can then be measured, indicating the interaction with an otherwise invisible particle, similar to how neutrinos are detected [22]. Examples for direct detection experiments are XENON1T [30], LUX [31, 32, 33], CRESST [34], DarkSide [23] and PandaX [35].

More details on direct detection experiments can be found in section 4.1.

1.5.3 Collider experiments

Figures 1.4 (c) and (d) show the production of dark matter particles at a collider experiment. Similarly to how a pair of dark matter particles can annihilate into two Standard Model particles, two dark matter particles can be produced from two Standard Model particles at sufficiently high energies at particle accelerators such as the Large Hadron Collider (LHC) at CERN [36]. Conventional detectors at collider experiments are not able to directly detect the DM particles, but their production can be inferred from missing transverse momentum (E_T^{miss}, $\not{E}_T$, or MET, for missing transverse energy) in the final state when having measured all other visible decay products [37]. However, not all invisible decay products are necessarily dark matter; for example the detectors at collider experiments cannot directly detect neutrinos, but the neutrino background can be derived well from the Standard Model [14].

Some more details about dark matter interactions at colliders can be found in the following section and section 2.1.1.

1.5.4 Mediator particles between Standard Model matter and dark matter

The nature of the interaction between Standard Model particles and dark matter particles is unknown as indicated by the "blobs" used to represent the interaction in figure 1.4. One possibility is that the interaction is mediated by another particle, similar to how the gauge bosons in the Standard Model propagate interactions. This is especially relevant for collider experiments as they could produce such a mediator (see section 2.1.1). The investigation of the interaction between dark matter and Standard Model matter is a specialty of collider experiments [14].

This mediator could be produced and observed in collider experiments as a resonance, a "bump", above the background centred around the invariant mass (rest mass) of the mediator if it decays immediately into Standard Model particles [11], as sketched in figure 1.5. This means that mediators between Standard Model matter and dark matter could be

discovered through their visible decays, and offer further evidence for physics beyond the Standard Model and dark matter, even without the need to measure and detect the dark matter particles themselves [10, 11]. However, when such a resonance is discovered, direct detection, indirect detection, and/or invisible collider searches are needed to determine whether this mediator is connected to dark matter.

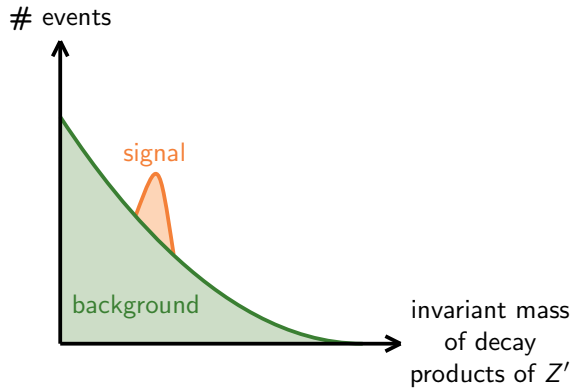

Figure 1.5: This sketch shows a "bump" above the expected background, indicating the production of a resonance particle.

It is possible that the Standard Model interacts with dark matter through the Z boson (Z portal models) of the weak interaction, or the Higgs boson (Higgs portal models) [14]. Additionally, there could be new types of dark boson mediators that couple to a dark sector that can include dark matter particles of one or more new species, such as WIMPs, depending on the model. For this, simplified models are used to describe the interaction with Standard Model particles. In a simplified model, all kinematic characteristics that are needed to design searches are included, but it is not necessarily a full theory (see also section 1.6). In such a simplified mediator model, the mediator can be a scalar, pseudoscalar (both with spin-0), vector or axial-vector (both with spin-1) boson, or a spin-2 mediator, each with just a small set of model parameters determining the masses and couplings of the mediator to Standard Model and dark matter particles [38].

Such an unstable mediator, a vector mediator called Z', similar to the Z boson of the Standard Model, is investigated here. More information about this model can be found in section 2.1.1.

1.6 The use of simple dark matter models

Many dark matter particle models are simple, but there are several reasons for why it is still interesting to look at such a simplified model. Firstly, the true nature of dark matter is unknown, so all dark matter models and interactions between dark matter particles and Standard Model particles are speculative within their constraints. It is therefore easier to start with a simple model that can be more easily extended and made more complex than an already complex model. It is likely that "simple" processes are discovered first, similar to how electrons and protons were first discovered as Standard Model particles, and more complex processes, like QCD, were discovered later. A figure to illustrate the steps of how the constituents of the Standard Model were historically discovered can be found in [39]. Furthermore, it is also hoped for that, at least most of, dark matter is simple in the way that it is only made up of one new type of particle.

Simple models also allow for broader searches, while complex models can make searches too specific so that other possibilities are not covered [14].

It might also be that only one "obvious" decay channel with one mediator plays a significant part in finding dark matter, similar to how many Standard Model particles were discovered first, especially when considering a single type of interaction, as it is the case with proton-proton collisions at the LHC [37].

Chapter 2

Tools and methods for relic density calculations

In this chapter and the following chapter 3, the relic density for a light vector mediator Z' is investigated. It is simulated using the software programs MadDM [40] and micrOMEGAs [41]. MadDM is a plugin of MadGraph [42], a computer program that simulates Standard Model and BSM processes. The relic density is computed for different mediator masses, dark matter masses and coupling constants to Standard Model particles as well as dark matter particles. Two different models are considered to obtain the current value of the relic density observed today: freeze-out and freeze-in. This chapter describes the tools and methods used to carry out the relic density computations, while the results are presented in chapter 3.

2.1 Theoretical background

2.1.1 The vector mediator *Z'*

Here, a simplified model of dark matter interactions with Standard Model particles through a single, massive vector mediator is considered [37, 38]. This mediator, denoted by Z', is a vector boson, meaning that it has spin 1, and is, similar to the Z boson in the weak interaction, an unstable particle with neutral charge. Depending on the model, its mass and coupling strength to other particles can vary. Here, the vector mediator is investigated for light masses (< 300 GeV) and small (< 1) coupling constants to Standard Model matter, while the coupling constant to DM is set to unity in most cases.

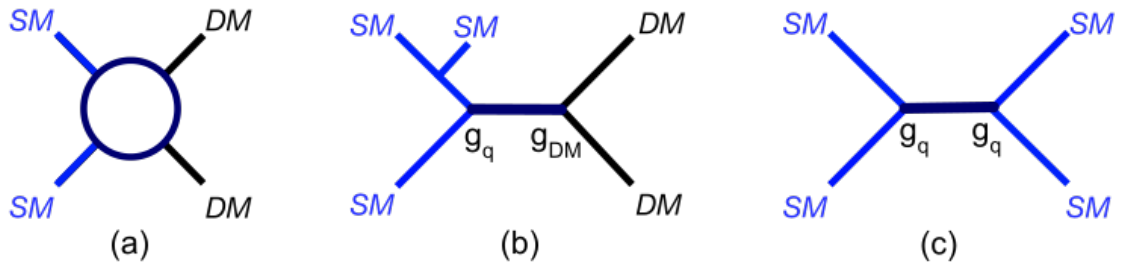

Figure 2.1: Diagrams to show the production of the mediator Z' from two Standard Model particles, the process at collider experiments, and its decay into either Standard Model particles (visible decays) or dark matter particles (invisible decays). Figure taken from [43].

At a collider experiment, the mediator could be produced in the collision of two Standard Model particles, which is sketched in the two diagrams (b) and (c) in figure 2.1. It can for example be produced from two quarks in proton-proton collisions as it is done at the LHC where the ATLAS experiment (see section 4.2.1) searches for this kind of signatures, as the mediator would be visible as a resonance (see sections 1.5 and 1.5.4). Since the protonic substructure consists of quarks, and at higher energies it is the constituents of composite particles that interact, the mediator can be produced from two quarks when the protons collide. Therefore, in order to create this kind of mediator in proton-proton

collisions, out of all Standard Model particles, the mediator has to couple at least to quarks.

Indicated in figure 2.1, after its production, the mediator can decay back into Standard Model particles, or dark matter particles, possibly WIMPs. Z' is assumed to decay immediately after its creation, so that it decays still inside the detector and does not escape it, and instead its decay products can be measured by detecting the produced Standard Model particles. If the mediator decays into invisible dark matter particles, its production is inferred from missing transverse momentum in the final state. This is possible because the energy and transverse momentum of the initial state are known. To conserve energy and transverse momentum, for each event, the sum of the four-momenta of all initial particles has to be equal to the sum of the four-momenta of all final-state particles[1]. As dark matter particles traverse the detector unnoticed, a discrepancy between the initial state and final state transverse momentum can indicate the production of dark matter. If the mediator decays into dark matter particles, an interaction in the initial state is required (figure 2.1 (b)) to be able to measure the transverse momentum. This can for example be a single jet (monojet) created from a gluon that is radiated off by one of the quarks.

The ability of the mediator to decay into dark matter particles also depends on its mass and the mass of the dark matter particles it can decay into. A mediator is *on-shell* when its mass is larger than the mass of the pair of dark matter particles it decays to, $m_{\text{med}} \geq 2m_\chi$, meaning that decays of the mediator into dark matter are energetically possible. If the mediator is *off-shell*, its mass is smaller than the mass of the dark matter pair, $m_{\text{med}} < 2m_\chi$, making decays into dark matter unlikely or impossible [45].

In this model, the mediator decays into only one type of dark matter particle. It is a Dirac particle, meaning that there exists an antiparticle that is different from the particle by an opposing electric charge [10, 44]. Therefore the pair of annihilating or produced dark matter particles consists of a particle and its antiparticle. Similar to the particles of the Standard Model that the mediator couples to, the dark matter particles are fermions.

The Lagrangian for the vector mediator is [38]

$$\mathcal{L} = -g_{\text{DM}} Z'_\mu \bar{\chi}\gamma^\mu \chi - g_q \sum_{q\,=\,u,\,d,\,s,\,c,\,b,\,t} Z'_\mu \bar{q}\gamma^\mu q - g_l \sum_{\ell=e,\mu,\tau} Z'_\mu \bar{\ell}\gamma^\mu \ell. \tag{2.1}$$

If interactions to neutrinos are also possible, the Lagrangian gains an extra term:

$$\mathcal{L} = -g_\nu \sum_{i\,=\,e,\,\mu,\,\tau} Z'_\mu \bar{\nu}_i \gamma^\mu \frac{1}{2}\left(1-\gamma^5\right)\nu_i \tag{2.2}$$

which is different from the term of the charged leptons since there are no right-handed neutrinos in the Standard Model, leading to parity violation in the interactions of the mediator with neutrinos [38].

The partial decay widths of the vector mediator are given by [38]

$$\Gamma^{\chi\bar{\chi}}_{Z'} = \frac{g^2_{\text{DM}}\, m_{\text{med}}}{12\pi}\left(1-4\cdot\frac{m^2_{\text{DM}}}{m^2_{\text{med}}}\right)^{1/2}\left(1+2\cdot\frac{m^2_{\text{DM}}}{m^2_{\text{med}}}\right) \tag{2.3}$$

$$\Gamma^{q\bar{q}}_{Z'} = \frac{g^2_q\, m_{\text{med}}}{4\pi}\left(1-4\cdot\frac{m^2_q}{m^2_{\text{med}}}\right)^{1/2}\left(1+2\cdot\frac{m^2_q}{m^2_{\text{med}}}\right) \tag{2.4}$$

[1]For a definition of four-vectors and four-momenta, see e.g. [10, 44].

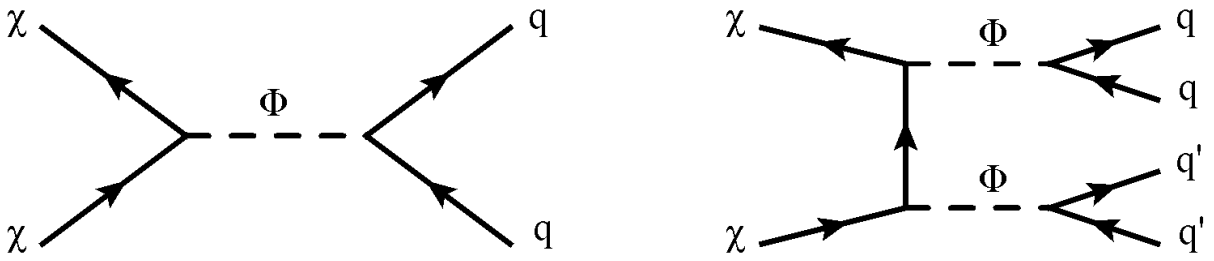

Figure 2.2: Diagrams showing the s-channel (left) and t-channel (right) annihilation processes. χ is a dark matter particle, Φ denotes the mediator, and q stands for quarks. Figure taken from [38].

$$\Gamma_{Z'}^{\ell\bar{\ell}} = \frac{g_l^2\, m_{\text{med}}}{12\pi}\left(1 - 4\cdot\frac{m_l^2}{m_{\text{med}}^2}\right)^{1/2}\left(1 + 2\cdot\frac{m_l^2}{m_{\text{med}}^2}\right) \tag{2.5}$$

$$\Gamma_{Z'}^{\nu\bar{\nu}} = \frac{g_\nu^2}{24\pi}\, m_{\text{med}} \tag{2.6}$$

for $m_{\text{med}} < 2m_{\text{DM},l,q}$. Depending on which fermions the mediator couples to, summing over the partial decay widths gives the total width of the mediator, Γ_{med}.

For this mediator, there are two important processes of how dark matter annihilates through the mediator into Standard Model matter. They can be seen in figure 2.2, where the left panel sketches the annihilation for the s-channel and the right panel for the t-channel.

The annihilation cross section σv for the s-channel is:

$$\sigma_s^V \cdot v = \sum_q \frac{N_c^q g_{\text{DM}}^2 g_q^2 \beta_q}{2\pi} \frac{2m_{\text{med}}^2 + m_q^2}{\left(m_{\text{med}}^2 - 4m_{\text{DM}}^2\right)^2 + m_{\text{med}}^2\Gamma_{\text{med}}^2}, \tag{2.7}$$

summed over all quarks with $m_q \leq m_{\text{DM}}$ and $\beta_q = \sqrt{1 - m_q^2/m_{\text{DM}}^2}$. $N_c^q = 3$ is the colour factor of the quarks, and v is the relative velocity between the two interacting dark matter particles.

For the t-channel, where $m_{\text{med}} \leq m_{\text{DM}}$, the annihilation cross section is

$$\sigma_t^V \cdot v = \frac{g_{\text{DM}}^4 \beta_{\text{med}}}{4\pi} \frac{m_{\text{DM}}^2 - m_{\text{med}}^2}{\left(m_{\text{med}}^2 - 2m_{\text{DM}}^2\right)^2} \tag{2.8}$$

with $\beta_{\text{med}} = \sqrt{1 - m_{\text{med}}^2/m_{\text{DM}}^2}$.

2.1.2 Dark matter relic density

The relic density of dark matter is a measure of the abundance of dark matter particles present in the Universe today. The currently observed value of the relic density is known from different astrophysical measurements of the CMB and is estimated to be about $\Omega_c h^2 = 0.12$ [16].

Similar to how the amount of Standard Model matter has changed with the evolution of the Universe, the abundance of dark matter was likely not constant in time. There are different hypotheses as to how the amount of dark matter could have developed to today's value. Two of these possibilities are considered here: the freeze-out scenario and the freeze-in scenario. Figure 2.3 illustrates how in each case the present relic density value is achieved.

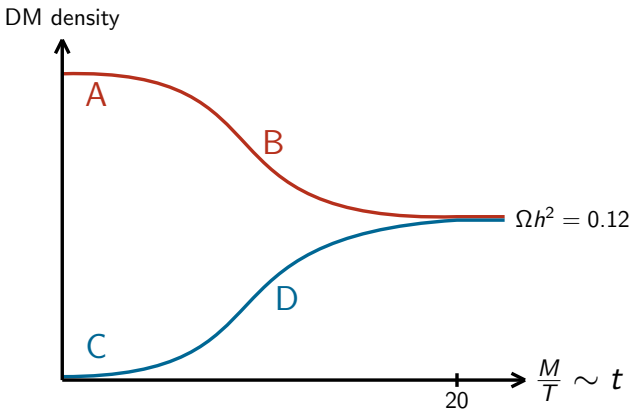

Figure 2.3: Sketch of the freeze-out and freeze-in process to obtain the currently observed value of the dark matter relic density. The upper (red) curve represents the freeze-out process, while the lower (blue) curve stands for the freeze-in mechanism. Over time, when the Universe cools, both processes approach the currently observed relic density value of 0.12, which occurs at around $M/T \approx 20$ [6].

Freeze-out mechanism

In the freeze-out mechanism, all dark matter is produced during the Big Bang, but the amount decreases with the evolution of the Universe. This process is shown in the upper (red) line in figure 2.3.

In the early Universe, when it is still dense and hot, the dark matter particles are in thermal equilibrium with the thermal bath from the visible sector (A). As the expansion rate of the Universe (Hubble rate) increases and becomes larger than the interaction rate of the dark matter particles with Standard Model particles, the dark matter particles decouple from the thermal bath. As the Universe expands and cools down (B), particle interactions become less likely, and the production of dark matter particles from high-energetic Standard Model particles ceases. Due to the reduced number density and energy of the dark matter particles, dark matter annihilation into Standard Model particles also becomes less likely. Similarly to how the amount of Standard Model particles approaches a certain value, the amount of dark matter approaches a constant value at about $m_{\mathrm{DM}}/T \approx 20$, where m_{DM} is the mass of a dark matter particle, and T the temperature of the Universe. This is the thermal, or freeze-out, relic density of dark matter [40, 46, 47].

Freeze-in mechanism

Another possibility for the production of the dark matter relic density is the process of freeze-in [47, 48, 49]. Conversely to the freeze-out mechanism, in the freeze-in model the abundance of dark matter is small in the beginning of the Universe but increases, and "freezes in" to the present relic density value.

The lower (blue) curve in figure 2.3 sketches this process. The initial amount of dark matter produced in the Big Bang is negligibly small (C). The dark matter particles only couple feebly to the thermal bath so that they never reach thermal equilibrium with the visible sector particles in the early Universe. As the Universe cools down, the dark matter number density increases due to the decay and annihilation of bath particles into dark matter particles (D). It is also possible that the interaction strength increases over time, leading to a higher dark matter production rate. Eventually, the abundance of dark

matter particles "freezes-in" to a constant value.

The dark matter particles produced from the freeze-in process are referred to as FIMPs ("Feebly-Interacting Massive Particles" or also "Frozen-In Massive Particles"), as opposed to WIMPs, emphasising their (initially) very small couplings to the thermal bath.

This can happen for more than one type of new particle, and mixed scenarios are possible. For example, the FIMP could not be the lightest stable particle in the dark sector, but instead the lightest stable particle could be produced from the FIMP through freeze-out, if the two species are in thermal equilibrium within the dark sector. This lightest, stable, massive particle would then be the dark matter particle [47]. In this work, only a simple case with one new dark matter particle is considered.

Reheating temperature

The temperature of Universe after the period of inflation is called reheating temperature. This is where dark matter production starts in the freeze-in case. There is no single theory of inflation and the constraints on the reheating temperature are not very narrow. The value of the reheating temperature places an important role in the energy of the (dark matter) particles when they first emerge, and thus strongly affects freeze-in processes. At larger reheating temperature, the particles have larger velocities which increases their interaction rate (see annihilation cross section σv in equation 2.7).

Typically, the reheating temperature is assumed to be large. For example, the default value in micrOMEGAs is set to $T_R = 3 \cdot 10^7$ GeV. Smaller temperatures are also possible. A constraint is given when considering that the reheating temperature has to be large enough to enable baryogenesis, i.e. it should not be smaller than 4 MeV [6, 50].

Since in the freeze-out scenario it is assumed that dark matter and Standard Model matter are in thermal equilibrium in the early Universe, changing the reheating temperature has no effect on the thermal relic density.

2.2 Method

The relic density produced by the Z' mediator decaying into dark matter can be calculated from simulations for a variation of mediator masses, m_{med}, dark matter masses, m_{DM}, coupling constants to Standard Model particles, g_{SM}, and coupling constants to dark matter, g_{DM}. The programmes used to calculate the freeze-out relic density are the plugin MadDM (version 2.0) of MadGraph, and micrOMEGAs (versions 5.0.2 and 5.0.9); whereas the freeze-in relic density is only computed in micrOMEGAs as MadDM does not offer a freeze-in option. In micrOMEGAs, the vector mediator model is found in the module called *ZpPortal*.

The aim is to investigate whether a model of DM with a light vector mediator, with masses below 300 GeV, can alone reproduce the relic density in the two scenarios. The initial choices of coupling constant values are based on what the LHC is currently sensitive to, and on what coupling values are reasonable for the relic density scenario (i.e. freeze-in usually requires small couplings).

2.2.1 Computation of the freeze-out relic density

To investigate the freeze-out relic density, MadDM and micrOMEGAs (version 5.0.2) are used for the same types of calculations, making it possible to compare the results.

For all computations, the ratio between the mass of the mediator and the mass of the dark matter particles is fixed to $m_{\text{med}} = 3 \cdot m_{\text{DM}}$. This choice is arbitrary and taken from the literature [51], and it is used to allow the mediator to decay to both DM and SM particles. The mediator mass is then varied between 10 GeV and 300 GeV, with a step size of 10 GeV.

The coupling constant between the mediator and the dark matter particles is fixed to unity, i.e. $g_{\text{DM}} = 1$. The coupling constant to Standard Model fermions is varied, ranging from $g_{\text{SM}} = 10^{-4}$ to $g_{\text{SM}} = 10^{-1}$ with a step size of 10^{-4}.

In the simplest case, the Standard Model couplings of the mediator are only couplings to quarks, since quarks are what the mediator Z' would be created from in collider experiments and the presence of quark decays is necessary for consistency. The coupling constant to quarks is denoted by g_q and is valid for all six quark flavours, meaning there is no distinction in the coupling value for the different quark types.

In some scenarios, couplings to leptons are also possible, where the lepton coupling constant is denoted by g_l. The relic density is computed for the following scenarios of Standard Model coupling constants. These benchmarks are taken from [38].

- g_q only
- $g_q = g_l$
- $g_q = 10 \cdot g_l$
- $g_q = 0.1 \cdot g_l$

Additionally, all three cases including couplings to leptons are performed with couplings to neutrinos and without. Similar to the quark couplings, all leptons couple equally to the mediator as they have the same coupling constant.

For the combination of different Standard Model matter coupling constants and mediator masses, the relic density is computed using the above mentioned programmes. The plots are produced from the simulated data using ROOT [52] with Python 2.7. A first plot is obtained with the mediator mass against the Standard Model coupling constant, while the relic density is displayed on a colour axis. Using interpolation between the data points to estimate the relic density values anywhere between the simulated points, a contour line is drawn for the relic density value of $\Omega_c h^2 = 0.12$, corresponding to the present dark matter abundance in the Universe. The contour line is obtained by using the `"CONT Z LIST"` drawing option of ROOT and `FindObject("contours")` to retrieve the contour.

2.2.2 Computation of the freeze-in relic density

The freeze-in relic density is computed using the freeze-in module in micrOMEGAs (version 5.0.9) [41, 49].

As the freeze-in mechanism is only well defined for light mediators and small coupling constants, the parameters need to be changed with respect to the freeze-out case [49].

First scans with a mediator mass of 10 to 50 GeV and coupling constants as in the freeze-out case strongly overproduced the relic density. Instead, to obtain the current relic density value, the mediator mass is fixed to a light mass and the parameters scanned are the Standard Model coupling constants as well as the coupling constant to dark matter. Thus the plots display the dark matter coupling and the quark coupling with the 0.12-contour line of the relic density.

Here, the Standard Model couplings always include couplings to quarks and leptons (with neutrinos). The step size of the coupling constant scans corresponds to the lowest displayed value in each plot.

Two cases are considered: on-shell, where the mediator mass is larger than the mass of the dark matter pair, and off-shell, where the mediator has a lighter mass (see also section 2.1.1). The mass of the on-shell mediator is fixed to 10 GeV and the previously used ratio between mediator mass and dark matter mass of $m_{\text{med}} = 3 \cdot m_{\text{DM}}$ is kept. Conversely, in the off-shell case, the dark matter mass is set to 10 GeV, and the relation between dark matter and mediator mass chosen to be $m_{\text{DM}} = 3 \cdot m_{\text{med}}$.

2.2.3 Changing the reheating temperature

In micrOMEGAs, the reheating temperature T_R is set by default to a relatively high value of $3 \cdot 10^7$ GeV, as this would be expected from theoretical models. However, no experimental evidence indicates that the value has to be that large [53]. Here, the freeze-in relic density for lower and varying reheating temperature is investigated. For this, either g_{SM} or g_{DM} are set constant, while the scan is performed over the other coupling constant and the reheating temperature. The SM couplings include all quarks and leptons (charged leptons and neutrinos). For all scans, the mediator is on-shell, with $m_{\text{med}} = 3 \cdot m_{\text{DM}}$ where $m_{\text{med}} = 10$ GeV.

Chapter 3

Results of the relic density computation

In this chapter, the results of the relic density computation for the light vector mediator described in chapter 2 are presented and discussed.

3.1 Results

In this section, all plots with the relic density of the vector mediator model are presented.

3.1.1 Freeze-out relic density with MadDM

The results for the freeze-out relic density computed with MadDM are presented in this part.

The relic density for which the quark couplings are the only possible couplings to Standard Model particles are shown in figures 3.1 and 3.2. Both plots display the mediator mass m_{med}, ranging from 10 GeV to 300 GeV, against the quark coupling constant, going from 10^{-4} to about 10^{-1}.

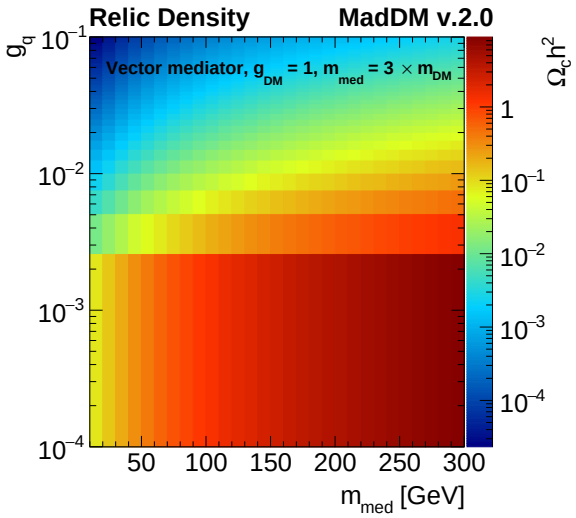

Figure 3.1: Freeze-out relic density for SM couplings to quarks only, and DM coupling to unity. Note that due to a ROOT plotting issue, the area for coupling below about 10^{-3} is not fully shown.

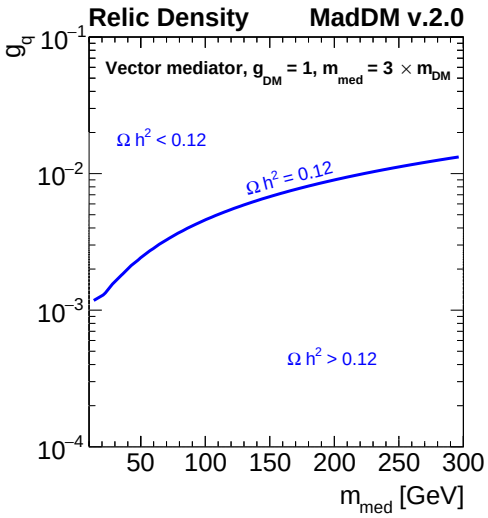

Figure 3.2: Contour line marking the currently observed value of the freeze-out relic density. Above the line, the value of the relic density is smaller, below the line it is larger.

Figure 3.1 shows the relic density $\Omega_c h^2$ on the z axis as a colour axis. The relic density values range from 10^{-2} (dark blue) to 10^{2} (red). The combination of larger couplings with smaller masses yields a smaller value of the relic density, depicted by the blue area, whereas the red area shows that the smaller the coupling but the larger the mass, the bigger the relic density becomes. The contour line for the currently observed relic density value of 0.12 is presented in figure 3.2. As the colour plot shows, the value of the relic density changes quickly when moving away from the 0.12-contour line.

The relic density contour lines for couplings to quarks as well as leptons with and without neutrinos are shown in figure 3.3. Similar to before, the area above each line denotes a smaller relic density value, and below the line a larger value.

The left panel of figure 3.3 shows the couplings to quarks and leptons but not including neutrinos. It can be observed that a small lepton coupling with respect to the quark coupling ($g_q = 10 g_l$, red line) effectively does not change the relic density compared to the quark-only case (blue line). For equal lepton and quark couplings ($g_q = g_l$, green line), there is a small decrease in the value of the relic density. When the lepton couplings are large with respect to the quark couplings ($g_q = 0.1 g_l$, violet line), the relic density is decreased.

In the right panel of figure 3.3, the contour lines of the lepton couplings including couplings to neutrinos are added as well. It can be seen that the neutrino couplings enhance the effect of the lepton couplings on the relic density already observed in the left panel, even if their impact is small.

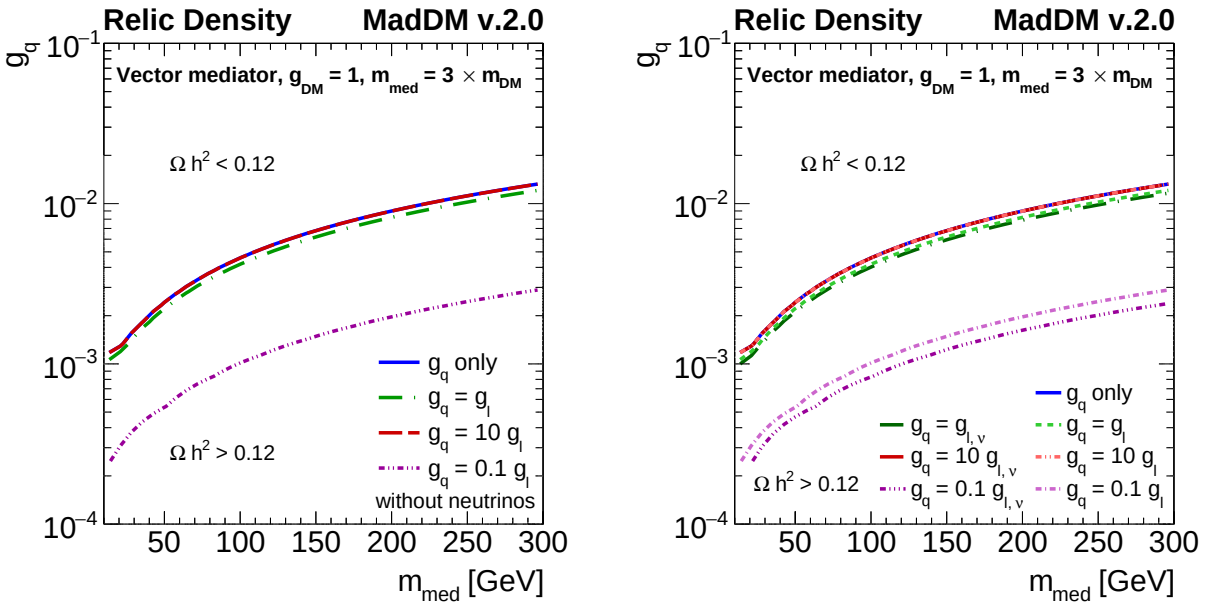

Figure 3.3: The 0.12-relic density contour line for different combinations of the quark and lepton couplings. In the left panels, the lepton couplings do not include couplings to neutrinos, while the right panel includes neutrinos in the lepton couplings where indicated.

Calculation of the dark matter annihilation cross sections

In the freeze-out scenario, dark matter annihilates into Standard Model matter over time, resulting in the relic density observable today (see also figure 2.2). The annihilation cross section σv is a measure of the probability of two dark matter particles χ to interact and annihilate (into the mediator). When computing the relic density, looking at the annihilation cross section can help to understand how the obtained relic density value is achieved. This means, for example, that if the annihilation cross section is very small, it is possible that not enough dark matter annihilates, resulting in a relic density value that is larger than the currently observed value.

To calculate the dark matter annihilation cross section for the vector mediator depending on its mass and the couplings to quarks, leptons and dark matter, equations

2.3 to 2.6 for the partial decay widths, and equation 2.7 for the s-channel annihilation process for quarks and leptons are used. Examples for the annihilation cross sections with different combinations of Standard Model and dark matter coupling constants are given in table 3.1 for a mediator mass fixed to 10 GeV.

Table 3.1: DM annihilation cross sections (s-channel) for $m_{\text{med}} = 10$ GeV.

coupling constants	σv [GeV^{-2}]
$g_{\text{DM}} = 1, g_{\text{SM}} = 10^{-5}$	$5.586 \cdot 10^{-13}$
$g_{\text{DM}} = g_{\text{SM}} = 10^{-5}$	$5.595 \cdot 10^{-23}$
$g_{\text{DM}} = 10 g_{\text{SM}} = 10 \cdot 10^{-5}$	$5.595 \cdot 10^{-21}$

3.1.2 Comparison of the freeze-out relic density with MadDM and micrOMEGAs

The 0.12-contour line for the quark-only case obtained with MadDM is plotted together with the result from micrOMEGAs in figure 3.4. The two lines are similar, only for a mediator mass below about 20 GeV, they start to diverge with micrOMEGAs producing a smaller relic density than MadDM. This was discussed with the micrOMEGAs team, but no resolution as to why this discrepancy occurs has been found yet.

For further comparison of the two results, table 3.2 presents a selection of relic density values from MadDM and micrOMEGAs for different mediator masses and a fixed quark coupling constant of $g_q = 2 \cdot 10^{-3}$. Looking at $m_{\text{med}} = 10$ GeV, it can be seen that the relic density in MadDM is more than twice as big as the value from micrOMEGAs. However, the values converge for larger mediator masses.

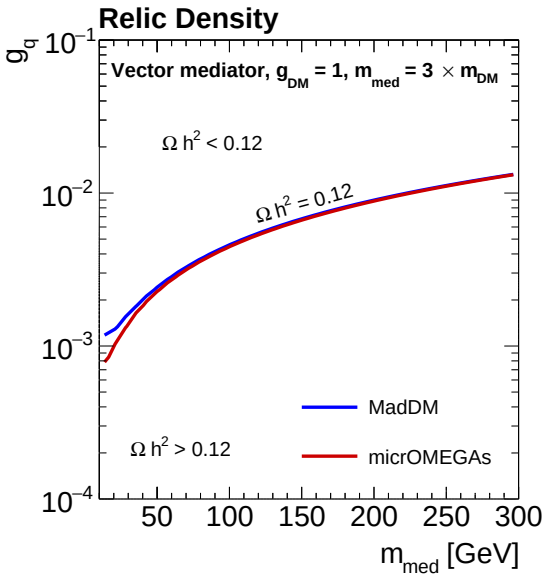

Figure 3.4: Freeze-out relic density contour for only quark couplings for MadDM (blue) and micrOMEGAs (red).

Table 3.2: Going along the line of the quark coupling $g_q = 2 \cdot 10^{-3}$, the corresponding value of the relic density from MadDM and micrOMEGAs is displayed for different mediator masses m_{med}.

m_{med} [GeV]	MadDM	micrOMEGAs
300	4.397	4.391
200	2.062	2.019
100	$5.758 \cdot 10^{-1}$	$5.462 \cdot 10^{-1}$
50	$1.714 \cdot 10^{-1}$	$1.518 \cdot 10^{-1}$
10	$3.631 \cdot 10^{-2}$	$1.486 \cdot 10^{-2}$

Plots including lepton couplings similar to figure 3.3 were created with micrOMEGAs as well, but are not presented here as the results are similar to what was obtained with MadDM.

3.1.3 Freeze-in relic density with micrOMEGAs

The results of the freeze-in relic density are presented here, first for the on-shell mediator case, then for off-shell.

The on-shell results are given in figure 3.5. The plots display the coupling of the mediator to quarks (g_q) against the coupling to dark matter (g_{DM}). Both couplings are very small, ranging from about 10^{-13} to 10^{-11}.

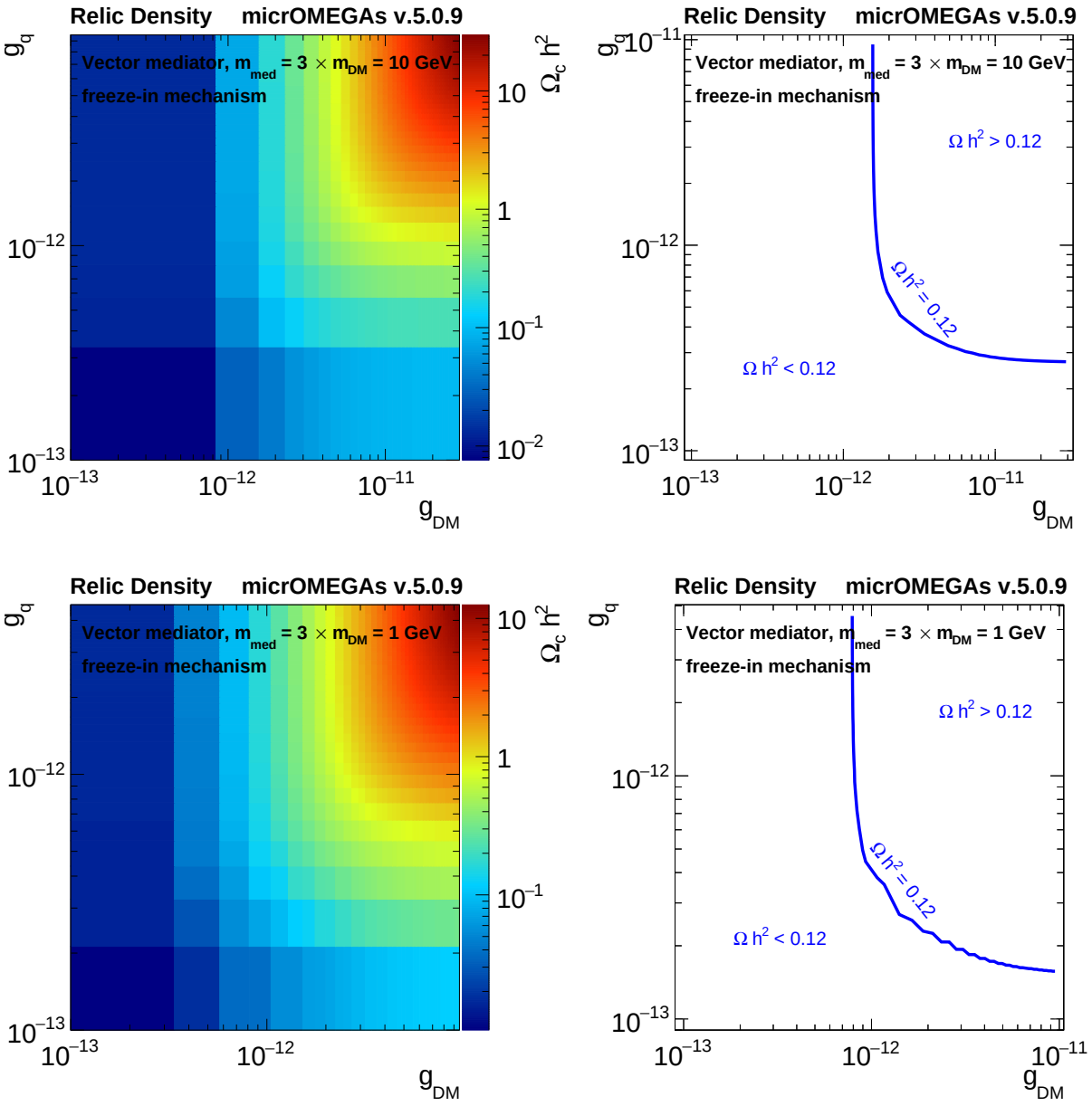

Figure 3.5: Freeze-in relic density for the on-shell mediator. The top panels show relic density with a mediator mass of 10 GeV, and the bottom panels a mediator mass of 1 GeV.

The two top panels show the relic density for a fixed mediator mass of 10 GeV, while

the bottom panels represent a mediator with mass 1 GeV.

The two left plots of figure 3.5 show the relic density on the z axis with values from $\Omega_c h^2 = 10^{-2}$ in the blue area, where both couplings are smallest, to about $\Omega_c h^2 = 10$ in the red area where the couplings are bigger, indicating a strong change in relic density when changing the couplings slightly. In the right plots, the corresponding 0.12-contour lines are drawn.

Figure 3.6 shows the results for the off-shell mediator. The dark matter mass is 10 GeV in the top panels and 1 GeV in the bottom panels.

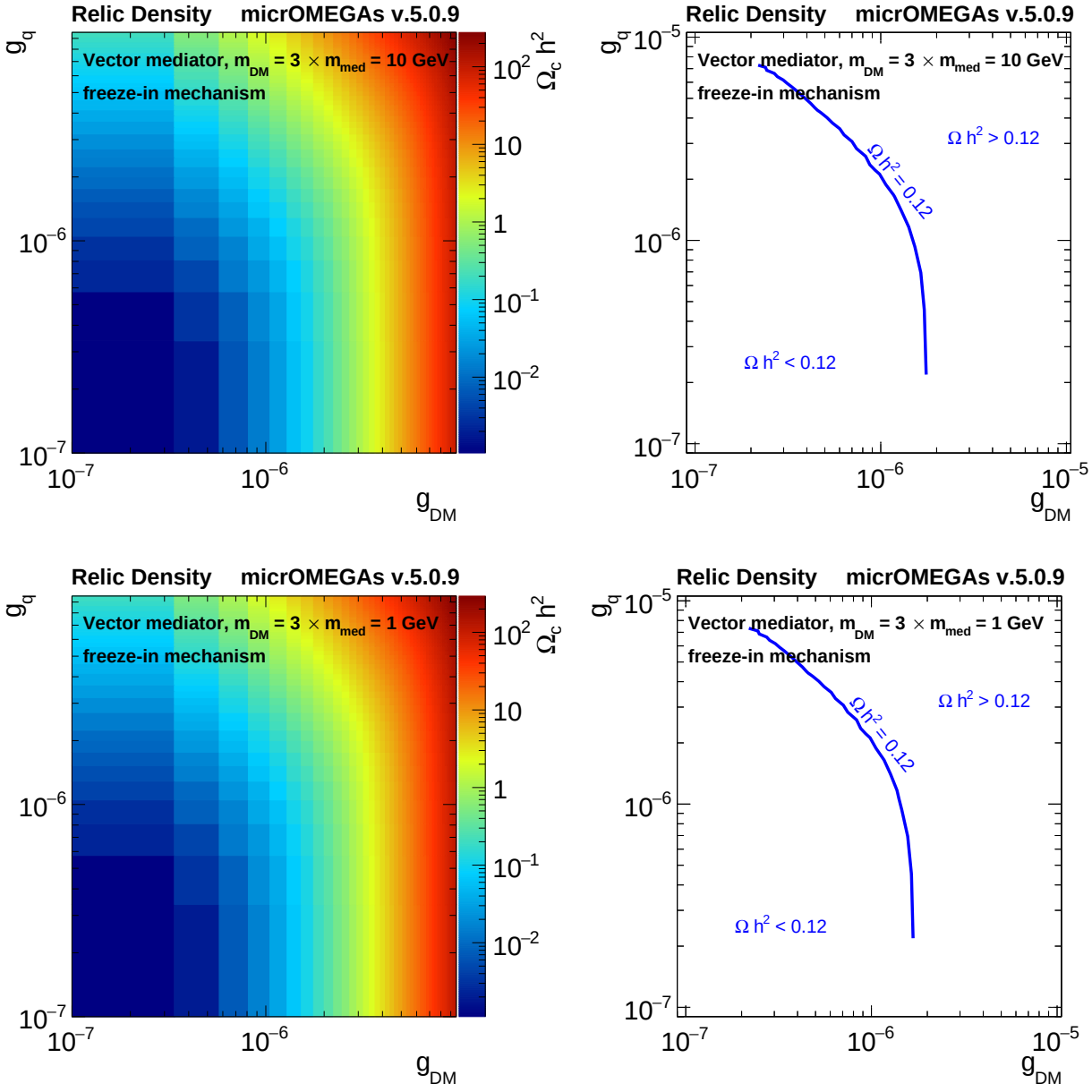

Figure 3.6: Freeze-in relic density for an off-shell mediator. The top panels show the relic density for a dark matter mass of 10 GeV, while for the bottom panels $m_{\mathrm{DM}} = 1$ GeV was used.

Both dark matter couplings and quark couplings (here equivalent to Standard Model couplings, meaning that all Standard Model fermions have the same coupling to the mediator) are in the order of 10^{-7} to about 10^{-5}. The relic density ranges roughly from 10^{-2} to 10^{2}, being smaller for a combination of small couplings (blue area) and bigger

for a combination of larger couplings (red area), indicating a fast change in relic density when changing the coupling constants by a few orders of magnitude.

For all cases in figures 3.5 and 3.6, the results are very similar, showing that for a mediator mass of a few GeV, the coupling constants to both dark matter and Standard Model matter have to be very small. Implications for the LHC sensitivity to this kind of scenario are discussed in section 3.2.

3.1.4 Freeze-in relic density for different reheating temperatures

Here, the results of the relic density for a varying reheating temperature are presented. In all plots, the mediator mass is on-shell and fixed to $m_{\text{med}} = 3m_{\text{DM}} = 10$ GeV.

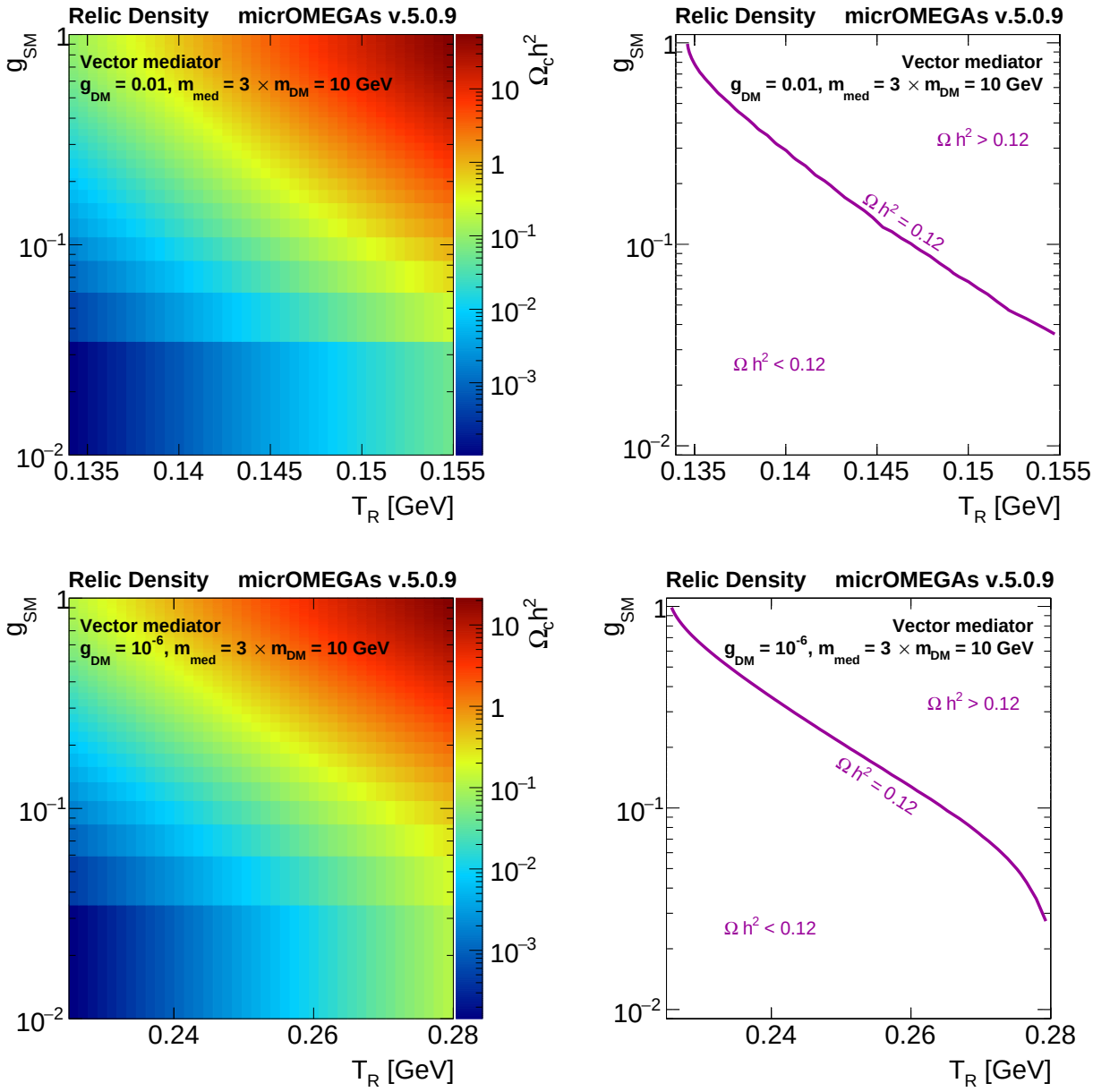

Figure 3.7: Freeze-in relic density for an on-shell mediator with dependence on the reheating temperature and SM coupling. Top panels: $g_{\text{DM}} = 0.01$. Bottom panels: $g_{\text{DM}} = 10^{-5}$.

In the first case, presented in figure 3.7, the dark matter coupling is kept constant,

while the Standard Model coupling varies. The top panels show the relic density for a DM coupling of $g_{\mathrm{DM}} = 10^{-2}$. For a SM coupling ranging between 1 and 10^{-2}, this reproduces the relic density for a range in reheating temperature of about 0.135 to 0.155 GeV. The relic density in the bottom panels is shown for $g_{\mathrm{DM}} = 10^{-6}$. This time, T_R ranges between about 0.22 to 0.28 GeV.

In both cases, the observed relic density is obtained for the combination of a smaller coupling and a larger reheating temperature, and vice versa. It can also be observed that the reheating temperature only varies slightly by a few hundred MeV, but that induces a large change in the relic density, as the wide range (4 to 5 orders of magnitude) of relic density values show.

In the second case, presented in figure 3.8, the SM coupling is fixed and the scan performed over the DM coupling constant in the range from 10^{-12} to 10^{-6}. The Standard Model coupling is set to 0.01 in the left panel, and 0.1 in the right panel. In both cases, the reheating temperature varies between about 0.5 and 2.5 GeV.

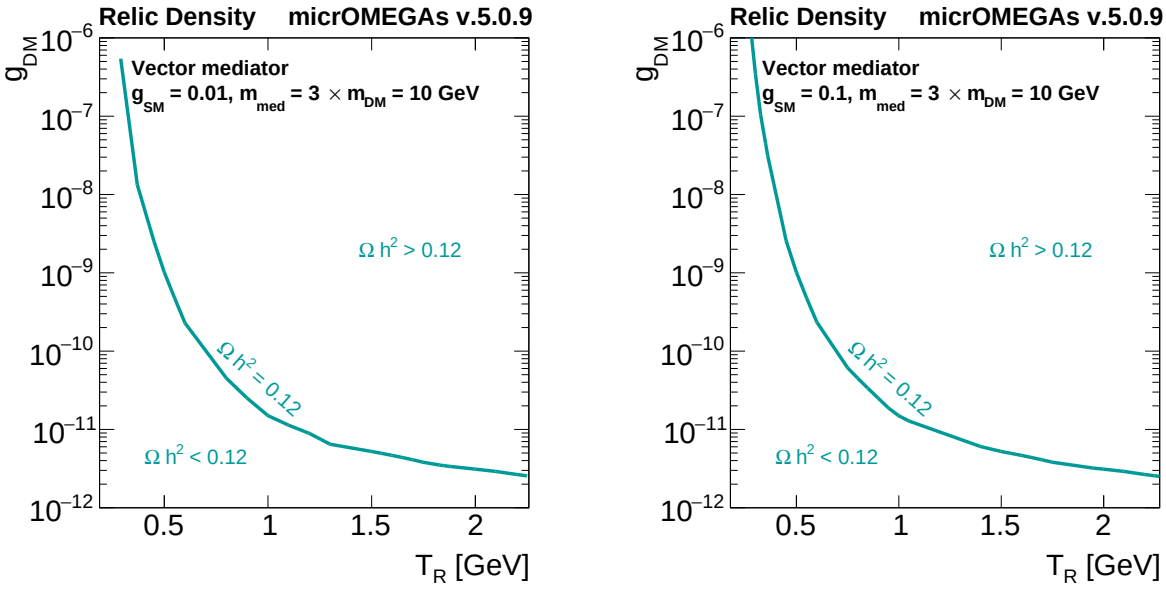

Figure 3.8: The 0.12-contour line of the on-shell freeze-in relic density with varying reheating temperature and dark matter coupling, for a constant Standard Model coupling of $g_{\mathrm{SM}} = 0.01$ (left panel) and $g_{\mathrm{SM}} = 0.1$ (right panel).

3.1.5 Freeze-in relic density with micrOMEGAs 5.0.2

Previously in this work, all freeze-in relic density calculations were carried out with micrOMEGAs 5.0.2. A bug was discovered by the micrOMEGAs team, affecting the freeze-in calculations corresponding to figures 3.5, 3.6, 3.7 and 3.8. With the fixed micrOMEGAs version 5.0.9, figures 3.5, 3.6 and 3.8 show no or negligibly little change to the previous version. Only the results of figure 3.7 differ. The relic density for the same ranges in Standard Model coupling and reheating temperature obtained with micrOMEGAs 5.0.2 is presented in figure 3.9.

It is noticeable that there is a turn in the relic density contour for a SM coupling at about $g_q = 0.5$. When increasing the coupling constant, the mediator width Γ increases since $\Gamma \sim g_{\mathrm{SM}}^2$ (see equations 2.3 to 2.6). The cross section is proportional to

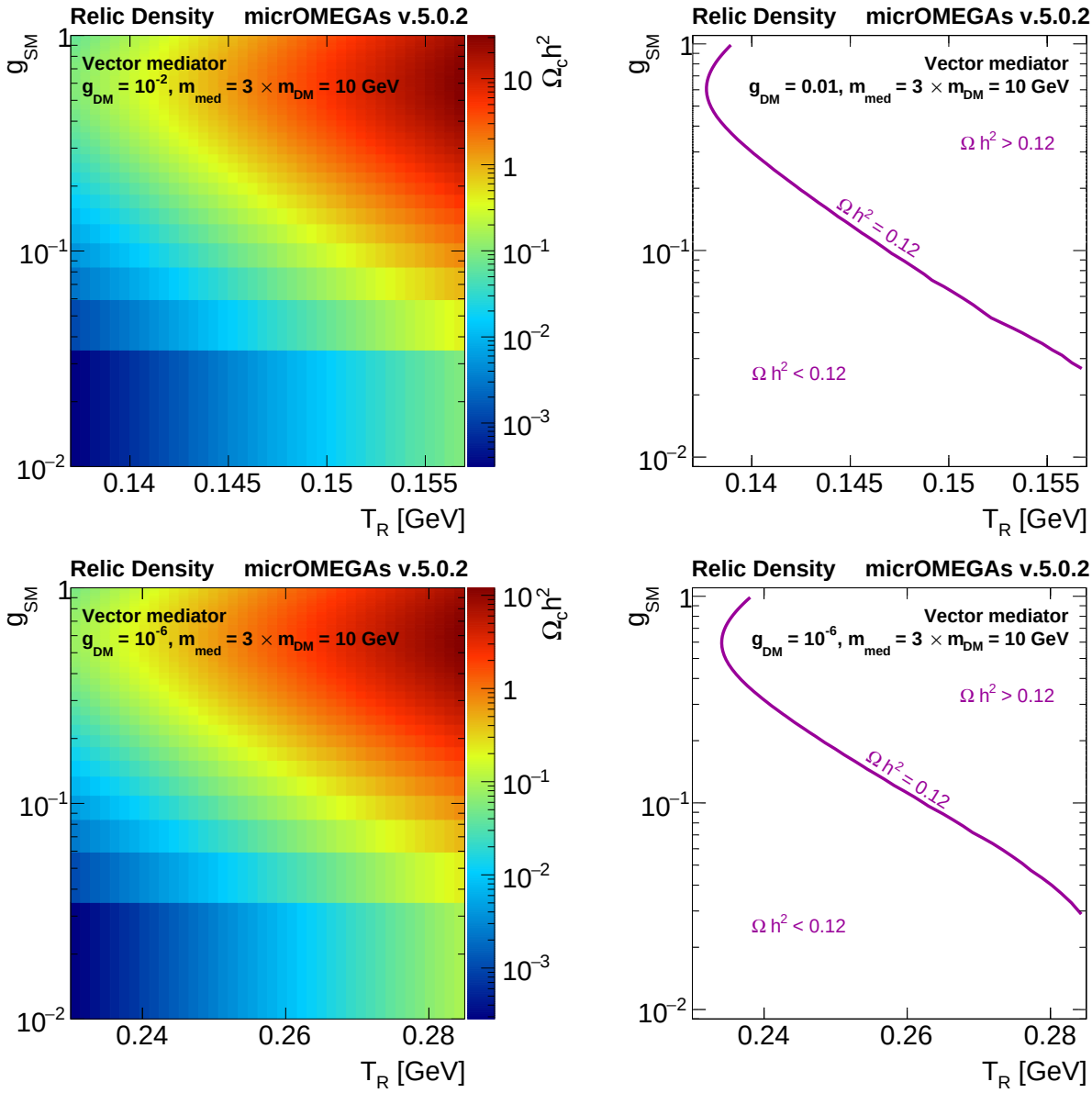

Figure 3.9: Freeze-in relic density for an on-shell mediator with dependence on the reheating temperature and SM coupling. Top panels: $g_{\mathrm{DM}} = 0.01$. Bottom panels: $g_{\mathrm{DM}} = 10^{-5}$.

$g_{\mathrm{SM}}^2 / \left((s - m_{\mathrm{med}}^2)^2 + m_{\mathrm{med}}^2 \Gamma^2 \right)$ (see equation 2.7, with $s = 4m_{\mathrm{DM}}^2$). When coming from below $g_{\mathrm{SM}} = 0.5$, the term $(s - m_{\mathrm{med}}^2)$ dominates over the term $m_{\mathrm{med}}^2 \Gamma^2$ that includes the mediator width. To maintain a similar amount of mediators, up to this point, the SM coupling increases as the reheating temperature decreases. At the turning point, the dominance shifts toward the latter term, $m_{\mathrm{med}}^2 \Gamma^2$, as now the coupling constant is large enough to give a width that is larger than the mediator mass. As $\sigma \sim 1/\Gamma^2$, the suppression of the mediator production is lifted by an increase in reheating temperature so that more mediators can be produced again.

In figure 3.7, this feature exists in both dark matter coupling cases as well, but it appears at a Standard Model coupling constant above 1 and is thus not included in these plots.

3.2 Discussion and conclusion

For all relic density plots it is important to notice that the contour line depicts the currently observed value of the relic density which in fact is the maximum value the relic density can take in order for the model to not be excluded as a dark matter candidate. Any relic density value above $\Omega_c h^2 = 0.12$ does not reproduce the astrophysical dark matter observations, and the model is not a viable candidate to explain DM in that region. However, the model is still valid for relic density values smaller than $\Omega_c h^2 = 0.12$. In this case, an additional dark matter contribution is required from other dark matter models to reach the desired amount of relic density. Thus a smaller relic density leaves the option to combine this vector mediator model with other dark matter models, as it is possible that dark matter consists of not just one type of new particle.

The different relic densities in the freeze-out scenario for different ratios between the quark and lepton couplings, presented in figure 3.3, show that a lepton coupling smaller than the quark coupling essentially has no impact on the relic density. For equal lepton and quark couplings, a small change is visible with the relic density being smaller than in the quark-only case. When the lepton couplings are larger than the quark couplings, a bigger impact arises and the relic density is even smaller; i.e. the 0.12-line is pushed towards smaller couplings and/or smaller mediator masses. Looking at the difference arising from lepton couplings including and excluding couplings to neutrinos, the effect of the additional couplings to neutrinos enhances the modification caused by the lepton couplings. This means that if the lepton couplings are larger than the quark couplings, they should not be neglected. Generally, the quark couplings have a stronger impact on the production and decay width of the mediator, as they contribute to the decay width by a factor of three more than the leptons. This is due to the colour charge of the quarks [37], see equations 2.4. Also, the quarks have on average larger masses than the leptons, which further increases their contribution.

According to the calculations of the dark matter annihilation cross section, presented in table 3.1, for this combination of small couplings and small masses the annihilation cross section becomes very small, which explains the overproduction and/or insufficient annihilation of dark matter for these small couplings and masses, and the large values of the thermal relic density. Thus, for either small couplings or small masses, the other parameter needs to be increased to obtain the correct relic density.

When comparing the results from MadDM and micrOMEGAs, the similarity of the quark-only thermal relic density curve from each simulation shown in figure 3.4 supports the reliability of both programs.

For all results obtained with the freeze-in mechanism, the combination of a relatively small mediator and dark matter mass (in the order of a few GeV) with very small Standard Model and dark matter couplings is needed to produce the 0.12-relic density curve, as is expected for the freeze-in scenario. The results in figure 3.5 show that for an on-shell mediator with a mass of a few GeV, the coupling constants to both dark matter and Standard Model matter have to be very small. When changing to smaller mediator masses (and DM masses), the features of the relic density remain the same, but the couplings have to be shifted to slightly smaller values.

In the off-shell case, both coupling constants have to be larger by about 6 orders of magnitude to produce the correct relic density value compared to the on-shell case. This is due to the decays into dark matter particles becoming unlikely since the mass of a dark matter pair is larger than the mediator mass. Hence, to obtain the same relic density

value, larger coupling constants are required to compensate for the low masses. In the off-shell case, almost no difference is visible between a dark matter mass of 10 GeV and 1 GeV.

In all cases, for these values, a detection of the mediator at collider experiments is unlikely as the production (and decay) rate is very small, and the signal would be too weak to be visible and statistically significant. Currently, LHC sensitivities include quark couplings down to about 0.1 and lepton couplings down to about 0.01 [14]. For an example, see figure 3.10 that shows sensitivities down to about $g_q = 0.04$ for light mediator masses in monojet searches. The blue line represents the freeze-out relic density.

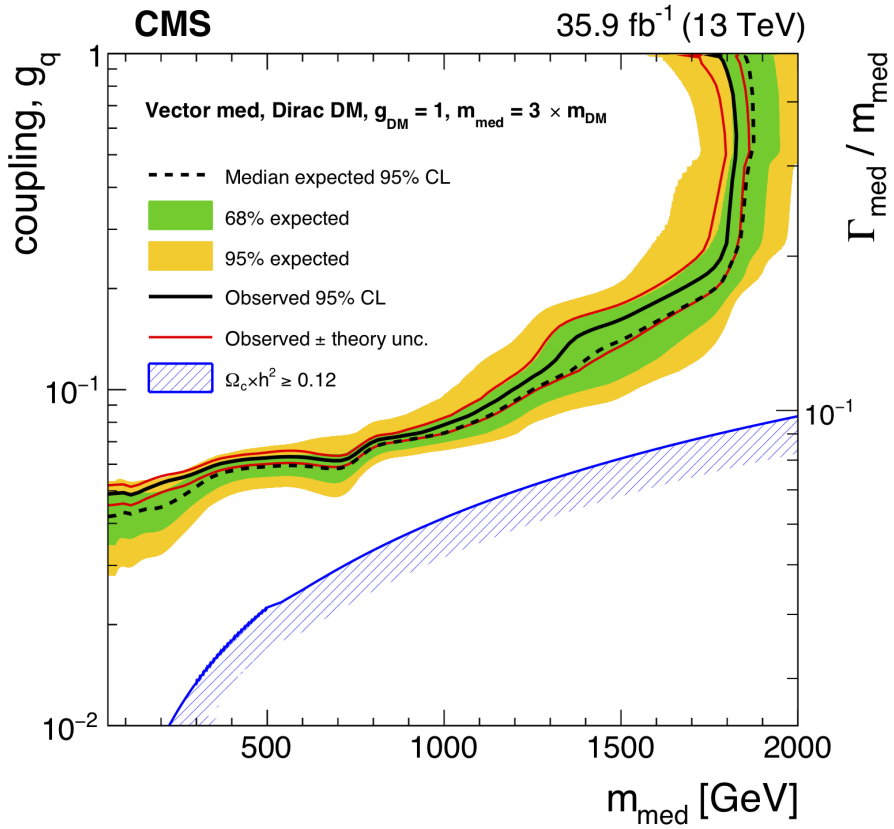

Figure 3.10: Results from the CMS mono-jet search. The plot shows current LHC sensitivity down to about $g_q = 0.04$ for this search. Plot taken from [51].

For the results of the scans over the reheating temperature it can be concluded that, in order to keep both SM and DM couplings close to unity, or at least reasonably close so that the interactions could be detected by experiments, the reheating temperature has to be very small. Since the reheating temperature is not well constrained, it is not possible to say how reasonable these small values are, and a wide range of values is possible. Additionally, it is shown that the range of reheating temperatures giving reasonable coupling values is very narrow, often just a few tens or hundreds MeV, before the resulting relic density becomes rapidly too large or too small. However, changing the reheating temperature to smaller values indicates that couplings large enough to be detectable at the LHC are possible for this mediator model.

Chapter 4

Dark matter constraints from LHC and direct detection experiments

Since the nature of dark matter is unknown, a large variety of experiments with different detection strategies is needed (see figure 1.4 and section 1.5). Indirect detection experiments search for (extra-)Galactic signals produced from annihilating dark matter, while direct detection experiments aim to detect dark matter particles that scatter with Standard Model matter, and colliders could produce dark matter particles. This work focuses on direct detection experiments and collider searches, but similar considerations and studies can be made for indirect detection searches. In this chapter and the following chapter 5, results from LHC searches and several direct detection experiment are discussed, focusing on astrophysical uncertainties in the direct detection results. After an overview (section 4.1) about the theoretical background of direct detection experiments, a summary of exclusion limits for both search strategies is shown and described (section 4.2). In section 4.3, the impact of a number of astrophysical uncertainties on the direct detection results is presented. The overall result is shown and discussed in chapter 5.

4.1 Direct detection experiments: detecting dark matter from Galactic sources

While collider experiments can produce dark matter particles, or the mediator, direct (and indirect) detection experiments can detect dark matter particles from Galactic sources. Direct and indirect detection experiments are necessary to confirm the cosmological origin of any discovery at the LHC. Built underground to avoid background signals from cosmic radiation, direct detection experiments search for WIMP dark matter particles interacting with the target material by elastically scattering off the nuclei (see also figure 1.4). It is the recoil energy from the collision with the dark matter particle that can be measured, which is expected in the order of keV [22]. The results of the direct detection experiments put constraints on the dark matter particle model in the plane of the WIMP-nucleon scattering cross section as a function of dark matter mass.

While the principle of dark matter interacting with SM matter is the same for all direct detection experiments, there are several detection principles. A common experimental setup for direct detection experiments are liquid noble-gas detectors, such as XENON1T [30, 54], LUX [31, 32, 33], DarkSide [23] and PandaX [35], where the noble gas acts as the target material. The CRESST experiment belongs to the detector type of cryogenic bolometers [22, 34].

In this work, mainly the results of LUX and XENON1T are investigated.

The XENON1T experiment

XENON1T is a direct detection experiment placed in Gran Sasso, Italy, searching for WIMP dark matter using liquid xenon [30]. It belongs to a series of experimental stages, starting with XENON10, an array of 10 tanks with 100 kg of liquid xenon each [55], and will be upgraded to XENONnT. First data from XENON1T was obtained in 2016. The

limit investigated here (figure 4.2) is from the XENON1T 2018 data [54]. No dark matter signals were found, leading to the exclusion limit.

The basic experimental setup can be seen in figure 4.1. The experiment is built as a time-projection chamber (TPC) and consists of a large tank with 2 tons of ultrapure liquid xenon as the target material, with photomultiplier tubes (PMT) below and above the target that detect scintillation signals created by an interaction with the target material. The brightness of the signal is a measure for the recoil energy deposited by incoming particles. Additionally, a second delayed signal is recorded by the PMTs from the ionised electrons during the interaction, since an electric field is applied to the tank. Obtaining two signals for each event makes it possible to determine the location of the interaction with an accuracy of a few millimetres. Background signals are expected from the decay of unstable xenon isotopes (e.g. ^{124}Xe), and therefore XENON1T is also an experiment on determining the half-life of unstable xenon isotopes. The main source of background comes from radioactive decays inside the detector, for example from ^{222}Rn and ^{85}Kr, as these cannot easily be removed from the xenon gas [30, 54, 56].

The 2018 results give dark matter exclusion limits for WIMP masses down to 6 GeV, and the lowest exclusion cross section is $4.1 \cdot 10^{-47}$ cm^2 at a mass of 30 GeV [54].

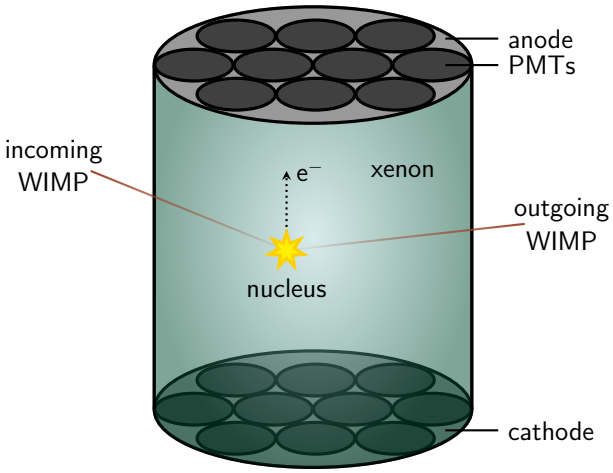

Figure 4.1: Sketch of a time-projection chamber (TPC) as used by the XENON1T and LUX experiments. An incoming WIMP interacts with one of the xenon nuclei in the tank. This creates two signals: the first one is a scintillation signal detected by the PMTs. The second signal, arriving slightly delayed, is an electric signal from the electrons that are freed during the interaction. Due to the electric field that is applied to the tank, electrons are attracted by the anode and measured by the PMTs. The WIMP leaves the detector.

The LUX experiment

The Large Underground Xenon (LUX) experiment [31] is a direct detection experiment at the Sanford Underground Research Facility (SURF) in South Dakota (USA) with first releases of data in 2013. Here (figure 4.2), results from 2017 are used as exclusion limit since no dark matter signal has been found [31].

LUX uses 250 kg of ultrapure liquid xenon as target material. The detector principle is a TPC with PMTs in the top and bottom of the tank, as sketched in figure 4.1. It can detect two kinds of signals for each occurring interaction: The first signal is a scintillation signal, while the second, delayed signal comes from the ionisation electrons that are freed

from the atoms during the scattering with the incoming particle. Due to this dual-signal, reconstruction of the incident location is possible. The ratio of the two signals is used to distinguish between recoils deposited on electrons and nuclei where the latter is expected for WIMP interactions. LUX is sensitive for nuclear recoil energies down to $E_R = 1.1 \cdot 10^{-6}$ GeV, corresponding to a dark matter mass of about 5 GeV [32, 33].

4.1.1 Calculation of event rates for direct detection experiments

In this section, an overview of the computation of event rates of direct detection experiments is given, as this will be useful to understand the assumptions and uncertainties involved.

The differential event rate for a direct detection experiment is calculated by

$$\frac{\mathrm{d}R}{\mathrm{d}E_R} = \frac{\rho_0}{m_{\mathrm{DM}} m_A} \int\limits_{v > v_{\mathrm{min}}} \frac{\mathrm{d}\sigma_A}{\mathrm{d}E_R} v f_{\mathrm{det}}\left(\vec{v}, t\right), \tag{4.1}$$

where E_R is the recoil energy of the nucleus in the target material after scattering with a dark matter particle, ρ_0 is the local (i.e. at the position of the solar system) dark matter density, m_{DM} and m_A are the masses of the dark matter particle and the nucleus, respectively, f_{det} is the velocity distribution in the detector rest frame, v the velocity of the dark matter particle, and $\mathrm{d}\sigma_A/\mathrm{d}E_R$ is the differential cross section of the DM-nucleus system,

$$\frac{\mathrm{d}\sigma_A}{\mathrm{d}E_R} = \frac{m_A A^2}{2\mu_p^2 v^2} \left(\sigma_{\mathrm{SI}} F_{\mathrm{SI}}^2\left(E_R\right) + \sigma_{\mathrm{SD}} F_{\mathrm{SD}}^2\left(E_R\right)\right), \tag{4.2}$$

where A is the atomic mass number of the nucleus, μ_p the reduced mass of the DM-nucleon system, i.e. $\mu_p = m_{\mathrm{DM}} m_A/(m_{\mathrm{DM}}+m_A)$, and σ_{SI} and σ_{SD} are the spin-independent (SI) and spin-dependent (SD) scattering cross sections. F_{SI} and F_{SD} are nuclear form factors describing the shape of the nucleus for SI and SD interactions, respectively. The spin dependence of an interaction depends on the type of mediator. For vector and scalar mediators, the scattering cross section is spin-independent. This means that there is no distinction between the interaction with protons and neutrons that the dark matter particle could interact with in the nucleus, and both types of nucleons give an approximately equal contribution, so it is referred to as DM-nucleon cross section. For axial-vector and pseudoscalar mediators, the interaction cross section is spin-dependent which requires a distinction between a scattering interaction with neutrons and protons [22, 45]. As this work focuses on a vector mediator, in the following only SI interactions are considered.

The "halo integral" is defined by

$$\eta\left(v_{\mathrm{min}}, t\right) \equiv \int\limits_{v > v_{\mathrm{min}}} \mathrm{d}^3 v \, \frac{f_{\mathrm{det}}\left(\vec{v}, t\right)}{v}, \tag{4.3}$$

and hence the differential event rate reduces to

$$\frac{\mathrm{d}R}{\mathrm{d}E_R} = \frac{\rho_0 A^2 \sigma_{\mathrm{SI}}}{2 m_{\mathrm{DM}} \mu_p^2} F^2\left(E_R\right) \eta\left(v_{\mathrm{min}}, t\right). \tag{4.4}$$

The minimum velocity a dark matter particle has to have to cause a detectable recoil energy E_R, which depends on the properties of the detector, is

$$v_{\min} = \sqrt{\frac{m_A E_R}{2\mu_A^2}}, \tag{4.5}$$

where here μ_A is the reduced mass of the DM-nucleus system [2].

In equation 4.4, one can set $C_{\mathrm{PP}} = A^2\sigma_{\mathrm{SI}}/2m_{\mathrm{DM}}\mu_p^2$, which represents all particle and nuclear physics dependencies of the event rate. The dependence on astrophysical quantities lies in the halo integral η and the local dark matter density ρ_0 [2].

The local velocity distribution of the DM particles with velocity $\vec{v}$ in the detector's rest frame is denoted as $f_{\mathrm{det}}(\vec{v}, t)$. It is normalised to unity, i.e.

$$\int \mathrm{d}v\, f_{\mathrm{det}}(\vec{v}, t) = 1, \tag{4.6}$$

for all possible DM velocities v.

Most commonly, the DM velocity distribution is assumed to follow a Maxwell-Boltzmann (MB) distribution which has the form

$$f_{\mathrm{MB}}(\vec{v}) = \frac{1}{\left(\pi v_0^2\right)^{3/2} N_{\mathrm{esc}}} \exp\left(-\frac{\left(\vec{v} + \vec{v}_\oplus(t)\right)^2}{v_0^2}\right), \tag{4.7}$$

where v_0 is the circular velocity at the position of the Sun, i.e. the velocity the Sun has in its orbit around the centre of the Galaxy, and $\vec{v}_\oplus(t)$ is the velocity of Earth with respect to the halo. The flux of dark matter particles incoming into the detector depends on the velocity of the detector, i.e. Earth. As Earth orbits the Sun, the velocity with respect to the galaxy and DM particle flux changes annually. Assuming a circular Earth orbit, $\vec{v}_\oplus(t)$ can be calculated by

$$\vec{v}_\oplus(t) = v_\oplus\left(\hat{e}_1 \sin(\lambda(t)) - \hat{e}_2 \cos(\lambda(t))\right), \tag{4.8}$$

where $v_\oplus = 29.8$ km/s is the orbital speed of Earth. The function $\lambda(t) = 2\pi(t - 0.218)$ modulates the yearly dependence on the Earth velocity, where t is given in units of years [6].

The vectors $\hat{e}_1$ and $\hat{e}_2$ span the plane in which Earth orbits. Given in Galactic coordinates, they are

$$\begin{aligned} \hat{e}_1 &= (-0.0670;\ 0.4927;\ -0.08676) \\ \hat{e}_2 &= (-0.9931;\ -0.1170;\ 0.01032)\,. \end{aligned} \tag{4.9}$$

According to [6], the motion of Earth can often be approximated by the solar velocity, $\vec{v}_\odot = (0, 220, 0)$ km/s.

The constant N_{esc} in equation 4.7 is a normalisation constant, given by

$$N_{\mathrm{esc}} = \mathrm{erf}\left(\frac{v_{\mathrm{esc}}}{v_0}\right) - \frac{2}{\sqrt{\pi}}\frac{v_{\mathrm{esc}}}{v_0}\exp\left(-\left(\frac{v_{\mathrm{esc}}}{v_0}\right)^2\right) \tag{4.10}$$

and v_{esc} is the escape velocity, i.e. the speed a particle needs to have in order to leave the gravitational potential of the Milky Way. It can be used as an estimate for the upper limit of the DM particle velocities, as particles with a larger velocity have likely escaped the Galaxy already [4] (see e.g. the analysis in section 4.3.4).

To obtain the total event rate R, the differential event rate (equation 4.4), is integrated over all recoil energies E_R and summed over all nuclei i in the target material,

$$R = \int \sum_i \epsilon_i (E_R) \frac{\mathrm{d}R_i}{\mathrm{d}E_R} \mathrm{d}E_R, \tag{4.11}$$

weighted by $\epsilon_i(E_R)$, the probability of detecting the recoil energy of a specific nucleus. For an exposure ε, the expected number of events is $\mathcal{N} = R\varepsilon$ [1].

4.1.2 The Standard Halo Model

Direct detection experiments require dark matter particles coming from space, and therefore they are dependent on the astrophysical properties of dark matter. The DM velocity and density directly affect the rate of incoming dark matter particles and thus the detection rate, i.e. the rate of recoil events of nuclei in the target material. Thus, the main sources of astrophysical uncertainties are the ignorance on the local DM density ρ_0, a measure of how the dark matter is distributed locally (i.e. in the solar system), on the velocity distribution of the dark matter particles $f(\vec{v})$, and in the unknown properties of the interaction between DM and the target nuclei, represented in the scattering cross section [1]. Therefore, knowledge about the rate and properties of incoming dark matter particles is important, as well as of their distribution in the solar system, to be able to interpret the experimental data. There may also be annual changes in the dark matter flux depending on the direction of Earth's motion around the Sun [6].

A common set of assumptions about these parameters is given in the Standard Halo Model (SHM). The SHM is a simplified model used to describe the dark matter properties in the Milky Way under the following assumptions [1, 2, 3]:

- The dark matter halo is spherical and isothermal, i.e. it is the same in all directions.
- The local dark matter density, i.e. the dark matter density at the position of the solar system, is assumed to be $\rho_0 = 0.3$ GeV/cm^3.
- To describe the velocity distribution of the dark matter particles, an isotropic Maxwell-Boltzmann distribution (equation 4.7) is used. Its peak velocity is set equal to the local circular velocity of the Sun, $v_{\mathrm{peak}} = v_0 = 220$ km/s.
- The Galactic escape velocity, i.e. the minimum speed a particle needs to have in order to escape the gravitational potential of the Milky Way, is assumed to be $v_{\mathrm{esc}} = 544$ km/s. This velocity can provide an estimate for the maximum velocity a dark matter particle could have.

These SHM assumptions are adopted by the direct detection experiments to produce the exclusion limits (see e.g. [54], or any of the direct detection references in figure 4.2). From the event rate (see equations 4.1 and 4.4), only m_{DM} and σ_{SI} are free parameters. For a known event rate, the data can thus be interpreted under the SHM assumptions to obtain the exclusion limits in the parameter space of DM-nucleon scattering cross section and dark matter mass.

However, these assumptions are prone to uncertainties, and making different assumptions can lead to a difference in the exclusion limit derived from the experimental data. This chapter and the following chapter 5 show, with inputs from several analysis groups, how alternative parameter choices can change the direct detection limits.

4.2 Summarising limits from LHC and direct detection experiments

Many experiments search for hints of particle dark matter. So far, no clear signal has been found. The null-results are summarised in exclusion plots, indicating where the investigated models are not backed up by experimental evidence. As so little about dark matter is known, determining what it is not is already helpful, and astrophysical constraints can guide the development of particle physics models and new search strategies. Combining data in one plot from complementary dark matter searches, such as collider and direct detection searches, and different experiments and searches from within each field, gives a broader picture and overview about what the properties of the interaction between dark matter and Standard Model matter might not be, and points to interesting regions to search for dark matter that are still uncovered. Figure 4.2 is such a summary plot, showing results from several LHC searches and different direct detection experiments. While direct detection experiments can detect the dark matter particles themselves and determine their abundance through the event rate, collider searches can show that there are invisible particles by producing them, and investigate properties of their interaction with Standard Model particles [14]. To obtain a full understanding of particle dark matter, these complementary searches are needed.

Exclusion limits from LHC searches are usually presented in a DM-mass–mediator-mass plane, while direct detection limits are shown in the DM-mass–scattering cross section parameter space. To combine limits from both search strategies into one parameter space, the LHC results are translated into the parameter space of the DM-nucleon scattering cross section against the DM mass [45]. To do this, the LHC limits are reinterpreted by calculating the DM-nucleon scattering cross section. For a vector mediator, the SI scattering cross section is

$$\sigma_{\mathrm{SI}} = \frac{f^2\left(g_q\right) g_{\mathrm{DM}}^2 \mu_{n\chi}^2}{\pi m_{\mathrm{med}}^4}, \tag{4.12}$$

where $f\left(g_q\right)$ describes the coupling between the nucleon and the mediator in dependence of the quark coupling. It is $f\left(g_q\right) = 3g_q$ for a vector mediator. The cross section becomes [45]

$$\sigma_{\mathrm{SI}} \approx 6.9 \cdot 10^{-41}\ \mathrm{cm}^2 \left(\frac{g_q g_{\mathrm{DM}}}{0.25}\right)^2 \left(\frac{1\ \mathrm{TeV}}{m_{\mathrm{med}}}\right)^4 \left(\frac{\mu_{n\chi}}{1\ \mathrm{GeV}}\right)^2, \tag{4.13}$$

where $\mu_{n\chi}$ is the reduced mass of the DM-nucleon system, $\mu_{n\chi} = m_n m_\chi/(m_n + m_\chi)$, making the cross section dependent on the dark matter mass. g_q and g_{DM} are constants and given by the model. The mediator mass enters corresponding to the dark matter mass, so that the LHC limits are translated in terms of DM mass and SI DM-nucleon scattering cross section [45].

The summary plot with LHC and direct detection searches is shown in figure 4.2, ranging in dark matter mass from 1 to 2000 GeV, and in cross section from 10^{-48} to 10^{-37} cm^2. As previously, the LHC results consider a vector boson as the mediator particle. The coupling constants are $g_q = 0.1$, $g_l = 0.01$ and $g_{\mathrm{DM}} = g_\chi = 1$. The LHC limits are given at 95% confidence level (CL) and the direct detection limits at 90%.

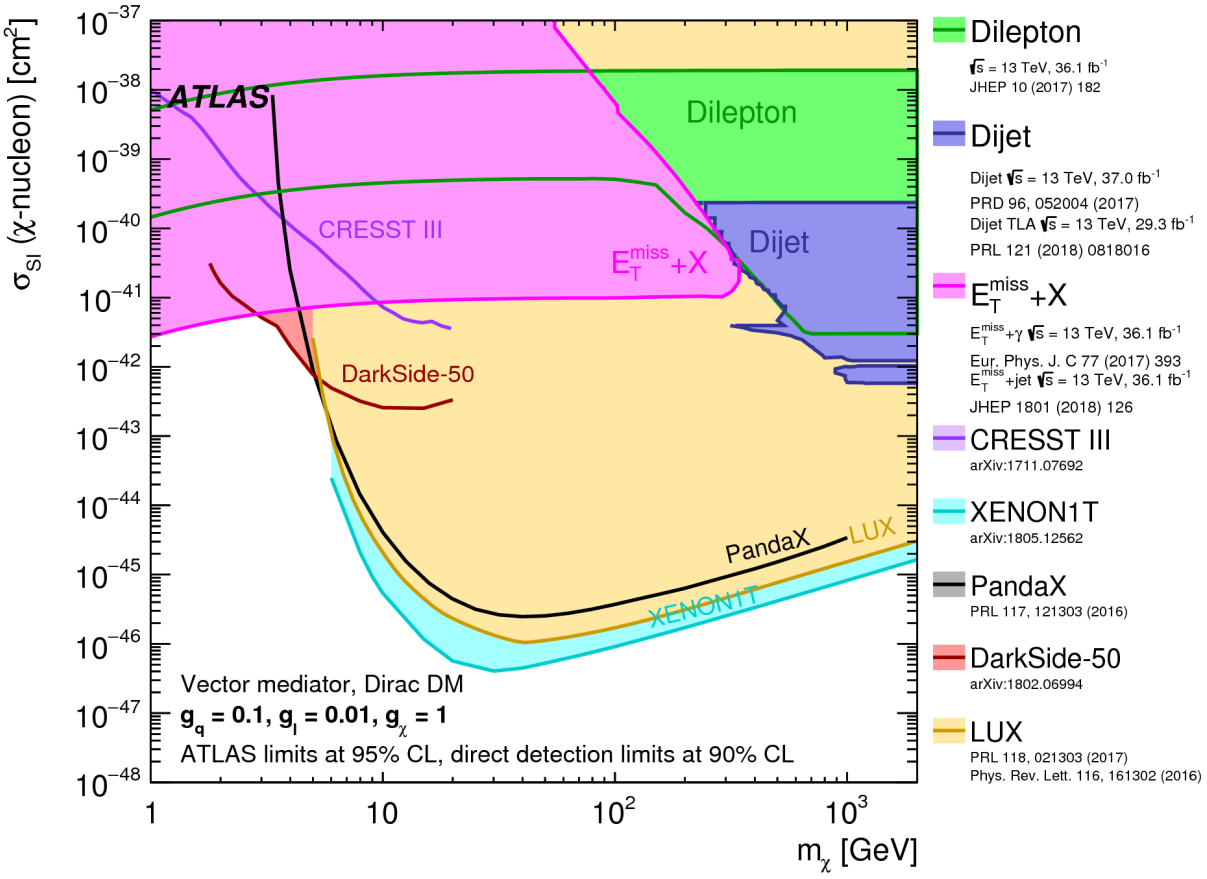

Figure 4.2: Plot [57, 58] summarising constraints on the cross section of the DM-SM interaction from LHC searches and direct detection experiments.

4.2.1 Limits from LHC searches

Figure 4.2 includes several searches sensitive to vector mediator models of DM from the LHC. The results shown are those from the ATLAS experiment (see below). Specifically included are dilepton searches [59], dijet searches at centre-of-mass energy $\sqrt{s} = 13$ TeV [60] and at trigger-level analysis (TLA) [61], as well as different $E_T^{\text{miss}} + X$ searches, where X corresponds to a single signal, such as a photon [62] or a monojet [63], and E_T^{miss} indicates invisible decays (see figure 2.1 (b)). These results from different channels can be directly compared [45], but the results are only valid for this type of model under the set assumptions of DM mass, mediator mass and coupling constants.

There are also experimental and theoretical uncertainties in these searches, but they are not shown in this plot.

The ATLAS experiment

The ATLAS (A Toroidal LHC Apparatus) experiment [64] is one of the main experiments at the LHC, operating since 2008 [11]. Located underground at CERN (Geneva, Switzerland) to shield the sensitive detectors from cosmic radiation, it is a general-purpose particle detector testing the Standard Model and searching for new physics beyond, such as SUSY.

A particle detector such as ATLAS whose purpose is to detect all kinds of fundamental

particles consists of many layers of different detector types, depending on the properties of the particles it should detect. The beam line goes through the centre of the detector where the particles collide. Parallel to the beam line, the ATLAS detector has a length of 44 m, while its diameter is 25 m [64]. In its centre, the two beams intersect, resulting in high-energetic particle collisions.

Closest around the beam line is the tracking detector, consisting of a silicon detector system and surrounded by a transition radiation tracker (TRT) that consists of drift chambers. This detector tracks electrically charged particles (e.g. electrons or protons) that are bent due to an applied magnetic field with a strength of 2 T [44]. The bent track makes it possible to calculate the momentum of these particles. The next detector type is the electromagnetic calorimeter that measures particles that can interact electromagnetically with the detector material. In the following layer, the hadron calorimeter, hadrons, i.e. particle composed of quarks, are detected through strong interactions in hadronic showers. The outer detector is a muon chamber that is used to track muons as they do not interact in the other detectors [6, 11].

Particles that only interact weakly, such as neutrinos, or WIMPs, do not interact in the detector and are thus invisible. Due to missing transverse momentum in the final state, their production can be inferred [10, 44].

Several trigger systems are used to store the events of interest. Selecting events according to desired criteria, as described in the individual references of the searches given above, results in different analyses such as the ones presented in figure 4.2.

4.2.2 Limits from direct detection experiments

The direct detection experiments in figure 4.2 are CRESST III, DarkSide-50, XENON1T and LUX. Their results can be valid for more than one model, unlike the collider constraints [45]. As the energies are lower than at collider experiments, direct detection experiments can use an effective theory to interpret the data where the interaction can be considered to be a contact interaction rather than an interaction mediated through a mediator [14].

While CRESST III and DarkSide-50 are more sensitive to lighter dark matter masses (below about 20 GeV), LUX and XENON1T are sensitive to dark matter masses up to 1 TeV and more. For smaller dark matter masses, i.e. 20 GeV and lower, the limits for PandaX, LUX and XENON1T weaken. In the case of this light dark matter, the mass of the dark matter particle is not large enough to enable the dark matter to deposit a recoil strong enough to be measurable by the experiments. Therefore the experiments only have a low sensitivity in this mass region. Additionally, it can be observed that the limits for PandaX, XENON1T and LUX move to larger cross sections for dark matter masses of about 50 GeV and more. As the total dark matter mass is fixed since the relic density is fixed, there are fewer dark matter particles when considering larger dark matter masses, leading to a lower rate at which dark matter particles could enter the detectors (see equation 4.4). Therefore, the detectors are less sensitive to larger dark matter masses.

4.3 Deviations from the standard Galactic assumptions in direct detection limits

The exact local DM density and DM velocity distribution of the dark matter halo of the Milky Way are unknown. Therefore, sizeable uncertainties can arise when estimating the event rate of direct detection experiments, since the event rate depends on how many particles traverse the detector and at what speed (see equation 4.4). Therefore it is important to investigate how assumptions of the dark matter halo affect the direct detection exclusion limits. Usually, the direct detection results can be rescaled linearly when assuming different local dark matter densities ρ_0 (see equation 4.4), but other uncertainties such as the velocity distribution do not enter as trivially [1, 4].

In this section, the results from four different analysis groups are presented using assumptions alternative to the SHM assumptions to interpret the results from direct detection experiments. Each analysis is briefly described and their uncertainty band shown. In the end, all exclusion limits and deviations are summarised in figures 5.1 and 5.2.

4.3.1 Uncertainties from the dark matter velocity profile

The following is a summary of parts of the analysis done in [1], focusing on how the uncertainties arising from the velocity distribution of the dark matter particles can be handled. In the paper, the method is described for the XENON1T 2017 data, but the uncertainty bands inserted in figures 5.1 and 5.2 are obtained with the 2018 data. Throughout this analysis, the local DM density is fixed to the SHM value of $\rho_0 = 0.3$ GeV/cm^3.

Analysis method

In the Standard Halo Model, it is assumed that the velocity distribution of the dark matter particles follows a Maxwell-Boltzmann distribution, which is given in equation 4.7 or, alternatively in this analysis,

$$f_{\mathrm{MB}}\left(\vec{v}\right) = \frac{1}{\left(2\pi\sigma_v^2\right)^{3/2} N_{\mathrm{esc}}} \exp\left(-\frac{\left(\vec{v}+\vec{v}_\odot\right)^2}{2\sigma_v^2}\right) \qquad \text{for } v \leq v_{\mathrm{max}} \tag{4.14}$$

with $v_{\mathrm{max}} = v_{\mathrm{esc}} + v_\odot$, and the velocity dispersion of the halo $\sigma_v \approx 156$ km/s.

However, deviations from this simple assumption are possible. There could be some dark matter substructures moving at different velocities in the form of dark matter streams or even a dark disk co-rotating to the stellar disk. These velocity perturbations can be added into the Maxwell-Boltzmann velocity distribution as velocity streams for which the velocity distribution is discretised, such that $f\left(\vec{v}\right) = \sum c_{\vec{v}_i}\delta\left(\vec{v}-\vec{v}_i\right)$, where $c_{\vec{v}_i}$ are the stream densities, ranging from 0 to v_{max}.

The deviation from the Maxwell-Boltzmann distribution is represented by the phenomenological parameter Δ,

$$\left|\frac{f(\vec{v}) - f_{\mathrm{MB}}(\vec{v})}{f_{\mathrm{MB}}(\vec{v})}\right| \leq \Delta, \tag{4.15}$$

where $f_{\mathrm{MB}}(\vec{v})$ is the Maxwell-Boltzmann velocity distribution and $f(\vec{v})$ the modified velocity distribution. If this equation equals zero, i.e. $\Delta = 0$, the SHM is restored. A

large Δ corresponds to a large deviation from the velocities assumed in the MB velocity distribution.

The adapted velocity distribution, $f(\vec{v})$, is normalised to unity,

$$\int_{v \leq v_{\max}} \mathrm{d}v^3 f(\vec{v}) = 1 \tag{4.16}$$

where $v_{\max}$ is the sum of the Galactic escape velocity v_{esc} and the velocity of the Sun with respect to the halo, $v_{\odot}$. Since the velocities range between $v_{\mathrm{esc}} = 499 - 608$ km/s and $v_{\odot} = 220 - 240$ km/s, the SHM case ($\Delta = 0$) contains an uncertainty as well.

The number of observed events (or less) is obtained from the p-value[1] of the cumulative Poisson probability distribution for a given dark matter mass, scattering cross section and DM velocity distribution. Then the p-value is optimised in the parameter space $(m_{\mathrm{DM}}, \sigma)$ of the direct detection results, by subjecting $\log p\,(m_{\mathrm{DM}}, \sigma)$ to equations 4.15 and 4.16 (i.e. determining $\log p\,(m_{\mathrm{DM}}, \sigma)$ so that these constraints are fulfilled).

For each Δ, the most conservative and the most aggressive limit are taken to obtain an uncertainty band in the cross section for a given dark matter mass.

Result

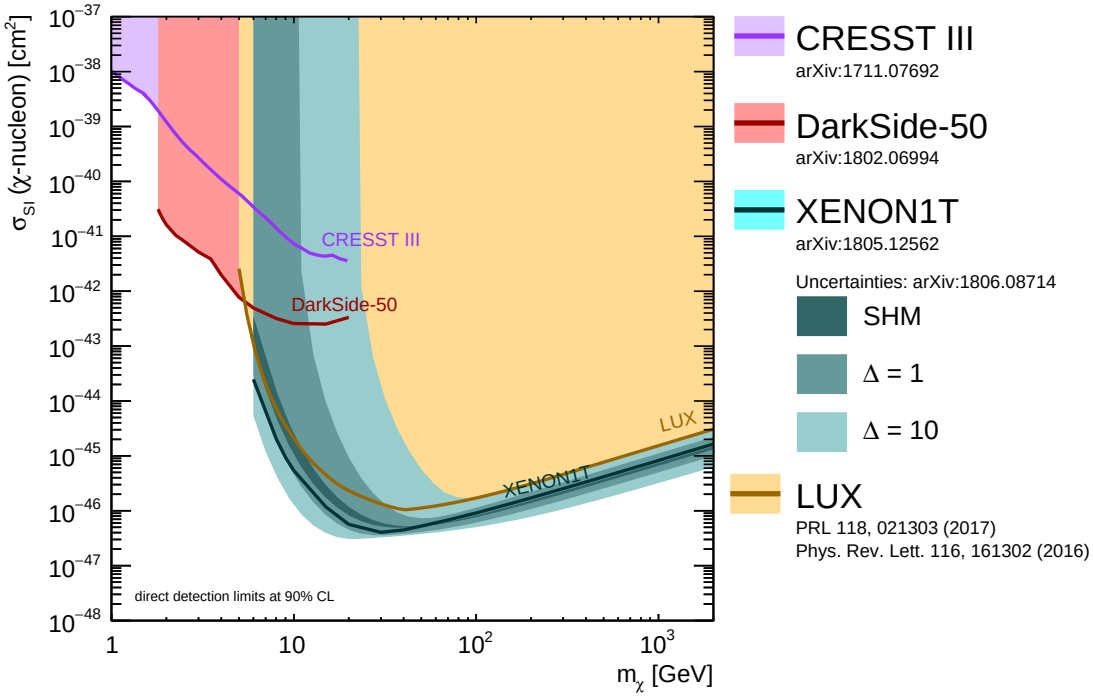

Figure 4.3: Direct detection exclusion limits with uncertainty bands around the XENON1T limit for deviations from the SHM assumptions. Uncertainties are given for $\Delta = 0$, which assumes SHM but includes uncertainties in the input parameters, $\Delta = 1$ and $\Delta = 10$.

The uncertainty bands shown in figure 4.3 correspond to values of Δ of 0 (SHM), 1 and 10. The larger Δ is, the larger the deviation in the velocity becomes, i.e. a larger

[1] Assuming the null-hypothesis is true, the p-value is the probability that the obtained result is as far away or farther than it is from the null-hypthesis [65]. For an expected number N_{BG} of background events and a number N_{sig} of expected signal events, the p-value is $p(N_{\mathrm{sig}}) = P(k \leq N_{\mathrm{obs}} \mid N_{\mathrm{BG}} + N_{\mathrm{sig}})$, where $N_{\mathrm{BG}} = 0.36$ for XENON1T [1].

Δ allows for more faster and slower velocities. Thus, the limits are absolute and are a measure of the velocity deviation from the standard assumptions. A larger Δ does not indicate a worse limit.

For light dark matter masses ($m_{\mathrm{DM}} \lesssim 25$ GeV), the uncertainty bands for $\Delta = 1$ and $\Delta = 10$ increase vertically, so that there is in principle no upper limit in the uncertainty for this mass region. This is due to the dark matter mass being so small that the energy transfer to the target nucleus in the detector is kinematically difficult, and also because for $\Delta \geq 1$, the optimal DM velocity distribution contains only dark matter particles with slow velocities. Therefore, the recoil energy deposited in the scattering is too small to be detected, and the limits degrade in this range.

For smaller dark matter masses, the stream velocity increases, resulting in an increase of momentum of the dark matter particles, which leads to larger nuclear recoil energies, eventually above the detectable threshold. However, since the stream velocity is bound from above by v_{max}, the experiment becomes insensitive for sufficiently small masses, as the momentum cannot increase any further.

4.3.2 Uncertainties from hydrodynamical simulations of Milky Way-like halos

This analysis [3] looks at simulated Milky Way-like dark matter halos and uses their local dark matter density and velocity distribution to interpret the direct detection data. This was done for the LUX data from 2013. Since figure 4.4 implements the LUX data from 2017, the curves from this analysis were rescaled to match the 2017 data, as suggested by the authors, and since the shape of the curve is not expected to change. The rescaling was done by determining the ratio between the exclusion limit from the 2013 data and 2017 data, and the obtained factor was multiplied to the curves from the 2013 data. The following is a summary of the analysis method from which the 2013 data uncertainty curves were gained.

Analysis method

Uncertainties in the properties of the dark matter halo arise from the ignorance on the density and velocity distribution of dark matter particles in the Milky Way. This analysis looks at dark matter halos similar to the Milky Way halo to investigate what alternative properties the Milky Way halo could possess.

From hydrodynamical simulations (APOSTLE and EAGLE), dark matter halos are generated. In this kind of simulations, hydrodynamics equations are used to simulate galaxy halos as a fluid made up of particles [66]. Then, halos that fulfil the known constraints on the Milky Way halo are selected. The conditions are that the rotation curve of the simulated halo has to fit well with the data from the Milky Way rotation curve, and that the stellar mass $M_\star$ of the simulated halo has to be within 3σ of the estimated stellar mass of the Milky Way, i.e. $4.5 \cdot 10^{10} < M_\star/M_\odot < 8.3 \cdot 10^{10}$, where $M_\odot = 2 \cdot 10^{30}$ kg is the solar mass.

For each of the selected halos, the dark matter density and the velocity distribution are extracted. This is done by using the halo integral (see equation 4.3), that can be factorised into the differential event rate of the direct detection experiment (equation 4.4) to accommodate for the changes. Then the new parameters are used to analyse the experimental data to obtain the exclusion limit.

Results

For this plot, curves of two different halos were included, shown in figure 4.4. A local dark matter density of $\rho = 0.3$ GeV/cm^3 was assumed for both so that only the velocity distributions differ from the SHM assumptions.

The halo labelled A1 has a peak velocity $v_{\text{peak}} = 223$ km/s, and, out of all the simulated MW-like halos, is the one with a peak velocity closest to the SHM value of $v_{\text{peak}}^{\text{SHM}} = 220$ km/s. It has a stellar mass of $M_\star = 4.88 \cdot 10^{10} M_\odot$.

The second halo, E3, is with $v_{\text{peak}} = 289$ km/s the halo farthest away from the SHM peak speed, and has a stellar mass $M_\star = 5.77 \cdot 10^{10} M_\odot$.

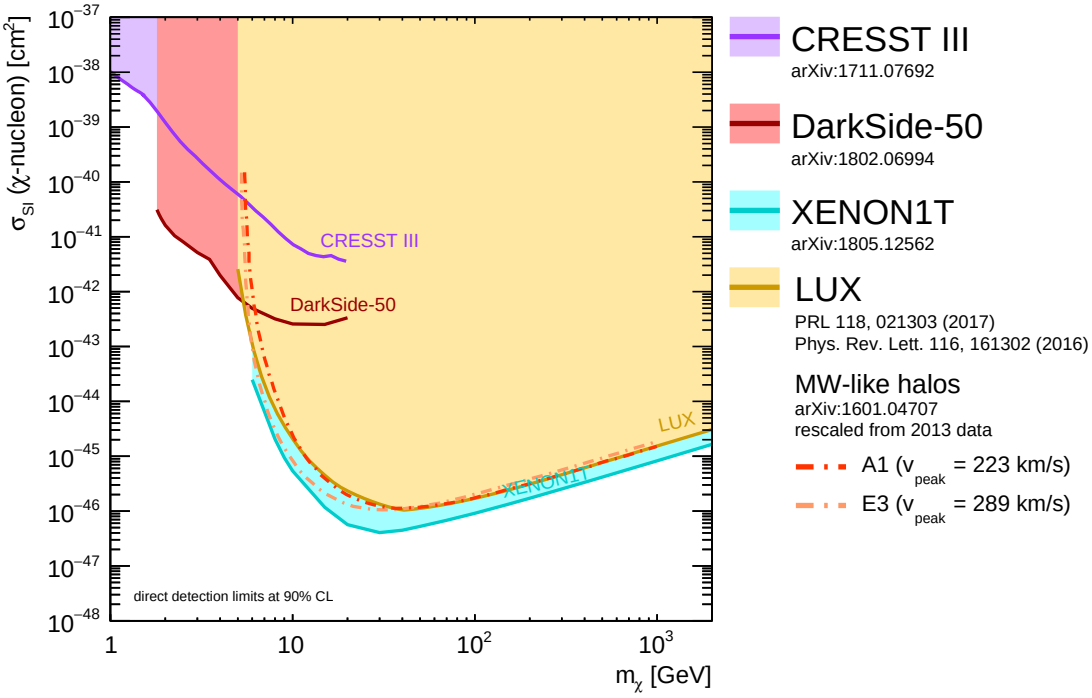

Figure 4.4: Direct detection exclusion limits with deviating LUX limits obtained from Milky Way-like halos. Results for two halos, both assuming $\rho_0 = 0.3$ GeV/cm^3, are included. The velocity distribution in halo A1 has a peak speed of 223 km/s, while halo E3 has a peak speed of 289 km/s.

4.3.3 Galactic uncertainties from visible matter components

When determining the dark matter content of the Milky Way, uncertainties in the dark matter density arise from uncertainties in the baryonic components[2]. This analysis [2] investigates how uncertainties from the visible matter affect the dark matter estimates. The analysis is done for the LUX 2015 data, but is rescaled (see explanation in the previous section) to match the LUX 2017 data in figure 4.5. The analysis method is briefly summarised in the following section.

Analysis method

To determine the dark matter density, the rotation curve of the Galaxy is observed. Measurements are taken for "tracer objects", i.e. objects with a circular orbit around the

[2] In astrophysics, baryonic matter includes atoms (but not photons or neutrinos) [9].

centre of the Milky Way to determine the gravitational potential of the Galaxy. Then this rotation curve is compared to the rotation curve that is expected from the visible matter components only. The discrepancy between the two rotation curves gives the dark matter content [2, 4].

For this, the visible components, i.e. the stellar bulge, the stellar disk and the interstellar medium (see figure 1.2 for a sketch) have to be accurately determined. The exact shape and distribution of these baryonic matter components are not exactly known, and choosing a model to describe the baryonic morphology affects the shape of the dark matter profile. Additionally, uncertainties arise from the ignorance on the solar properties, such as its distance from the Galactic centre that it estimated to be around $R_0 \approx 8$ kpc, and the local circular speed of the Sun, $v_0 \approx 220$ km/s.

To describe the Galactic dark matter distribution, this analysis adopts a generalised Navarro-Frenk-White (NFW) profile,

$$\rho_{\mathrm{DM}}(R) = \rho_0 \left(\frac{R_0}{R}\right)^{\gamma} \left(\frac{R_s + R_0}{R_s + R}\right)^{3-\gamma}, \tag{4.17}$$

with the local DM density ρ_0, the scale radius of the DM density profile R_s, that is kept constant here, and the profile index γ, where $\gamma = 1$ gives the standard NFW profile [2].

This is used to fit a specific baryonic morphology (i.e. combination of stellar bulge, disk and gas) and varying parameters R_0, v_0 and $M_\star$. From this, ρ_0 is determined, which is then used to interpret the direct detection results. The escape velocity is here assumed to be $v_{\mathrm{esc}} = 533$ km/s.

Result

While the analysis looks at different baryonic morphologies, figure 4.5 shows the uncertainty taken from only one morphology but with three different sets of Galactic parameters which are summarised in table 4.1. A larger dark matter density results in a lower exclusion limit, and the large variation in the dark matter density in the three curves is the main reason for the large deviation in the curves from the limit provided by the LUX experiment.

Table 4.1: This table summarises the varied parameters in the uncertainty curves shown in figure 4.5. The parameters are the distance from the Galactic centre to the Sun, R_0, the Sun's local circular velocity, v_0, the stellar mass of the Galaxy, $M_\star$, given in $10^{10} M_\odot$ where $M_\odot \approx 2{\cdot}10^{30}$ kg is the mass of the Sun, and the resulting local dark matter density ρ_{loc}.

curve	R_0 [kpc]	v_0 [km/s]	$M_\star$ [$10^{10} M_\odot$]	ρ_0 [GeV/cm^3]
upper	8.5	180	5.1	0.055
middle	8	230	4.6	0.466
lower	7.5	312	4.2	1.762

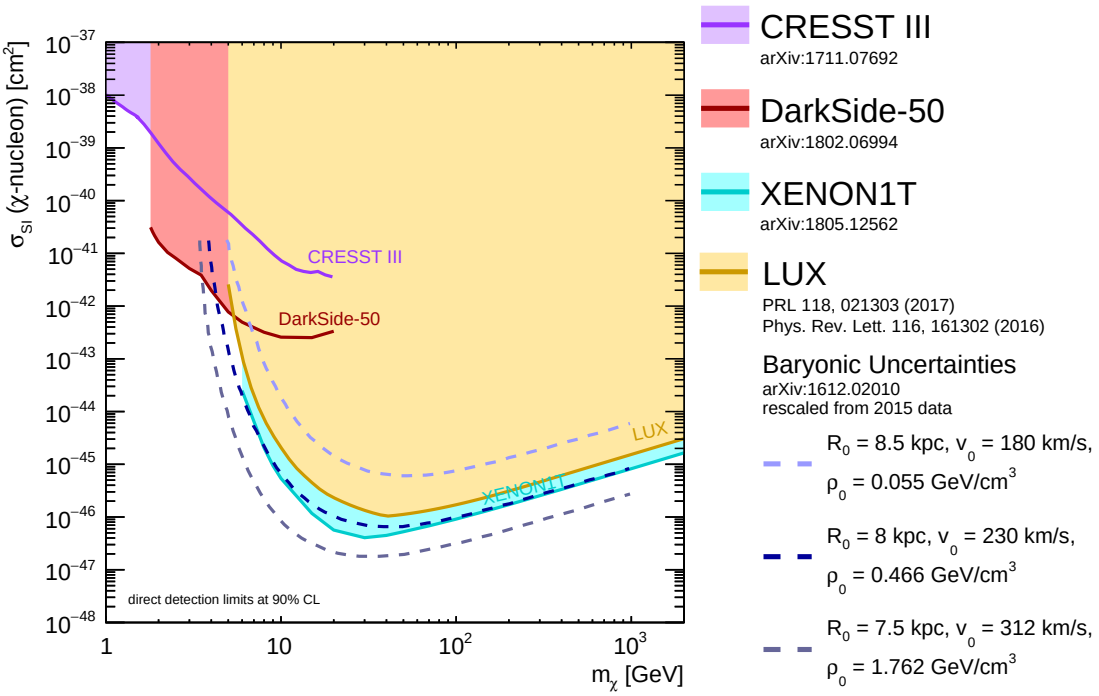

Figure 4.5: Direct detection exclusion limits with deviating LUX limits due to uncertainties in the baryonic Milky Way components. Each of the three curve represents a different choice of R_0, v_0 and ρ_0, as with values indicated in the legend.

4.3.4 Uncertainties from the dark matter distribution

This analysis [4] looks at the same uncertainties as the previous analysis in section 4.3.3, focusing on the ignorance on the exact dark matter distribution, due to the ignorance on the exact shape and content of the baryonic Milky Way components. The following is a brief summary of parts of the analysis in [4].

Analysis method

Using the rotation curve method (see explanation in previous section), the dark matter density distribution can be obtained assuming a NFW profile (see equation 4.17). However, the uncertainties on the baryonic components and the uncertainty on the position of the Sun set uncertainties on the dark matter density profile. To take these uncertainties into account, a likelihood profile is created. Specifically, the likelihood profile includes $R_0 = [7.5, 8.5]$ kpc (this affects v_0, since $v_0 = v(R_0)$, where the uncertainty in v_0 gives the uncertainty in the Maxwell-Boltzmann velocity distribution), $v_{\text{esc}} \approx [400, 700]$ km/s, and $\rho_0 \approx [0.08, 1.96]$ GeV/cm^3. For each combination of these three parameters a χ^2 uncertainty is given in the likelihood profile. From this, and following the instructions by the authors [67], an uncertainty band can be calculated for the direct detection limit. Details on the procedure can be found in appendix A.

Result and discussion

Following the instructions in [67], an uncertainty band for the LUX exclusion limit was computed [68]. It is shown in figure 4.6.

For dark matter masses below about 7 GeV, no results are available. This is because for small dark matter masses, the velocity of the particles has to be larger than for larger dark matter masses in order to deposit a recoil energy large enough to be picked up by the detector. For these small dark matter masses, the minimum velocity (equation 4.5) that the particles need to have is larger than the escape velocity of the best fit value given in the likelihood profile provided by the analysis group. This results in a negative and thus unphysical halo integral (see equations 4.3 and appendix A). The escape velocity of the best fit is $v_{\text{esc}} = 401$ km/s, which is relatively small compared to the SHM assumption of 544 km/s (see section 4.1.2). According to the results in [69], the escape velocity adopted by this analysis is likely an underestimation. For example, the analysis in the previous section 4.3.3 assumes a larger escape velocity ($v_{\text{esc}} = 533$ km/s), and does not have the problem that the minimum velocity becomes larger than the escape velocity for light particles.

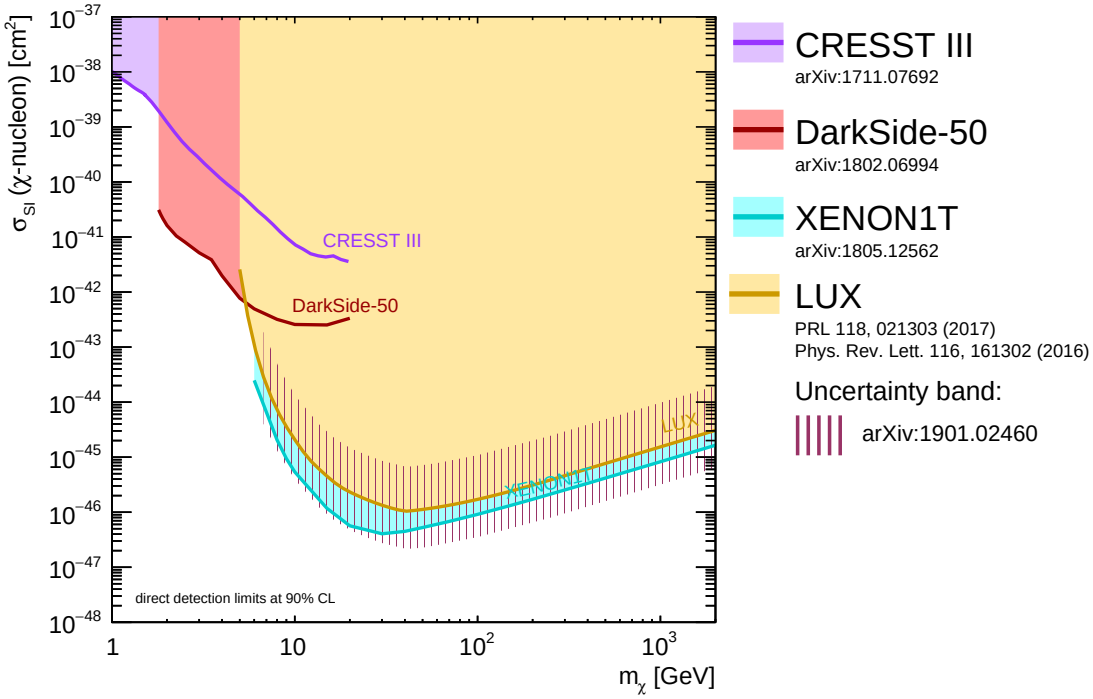

Figure 4.6: Direct detection exclusion limits with an uncertainty band for LUX from uncertainties in the dark matter distribution.

Chapter 5

Results and discussion of direct detection limits

5.1 Results and discussion

While the uncertainty curves of each analysis are individually shown in the corresponding sections in chapter 4, here they are summarised in one plot. Figure 5.1 presents the direct detection limits with the deviations and uncertainties from all four analyses, while figure 5.2 additionally includes the LHC searches. There is one set of uncertainties for XENON1T and three sets for LUX.

The different curves and bands show that the direct detection limits strongly depend on the astrophysical assumptions – the local dark matter density and velocity distribution – and can shift by up to about one order of magnitude in cross section when choosing extreme uncertainties in the astrophysical dark matter parameters.

The analyses in 4.3.1 and 4.3.4 both have problems when producing bands for small dark matter masses. While in the first analysis, the limits degrade due to the modified velocity distribution favouring small velocities that would be too small to deposit a detectable recoil energy for light dark matter particles, the second analysis excludes this mass range since the required minimum velocity would be larger than the Galactic escape velocity. This emphasises that for smaller dark matter masses, the dark matter particles can be more difficult to detect, so even more sensitive detectors are required, especially if the dark matter velocity is also slow.

5.2 Conclusion

The different analysis groups whose results are summarised in figures 5.1 and 5.2 have shown that different assumptions about the Galactic parameters (local DM density, DM velocity distribution, baryonic components), can affect the interpretation of the data from direct detection experiments and shift the exclusion limits with respect to the SHM assumptions. The results for the different analyses indicate that the uncertainties increase more for smaller dark matter masses, where the particle velocity becomes more crucial. Especially if the dark matter particles are both light and slow, LUX and XENON1T are currently less suitable to detect these particles.

These results also emphasise how much particle physics dark matter searches rely on the results obtained from astrophysical dark matter searches, and vice versa. Therefore, when looking at direct detection exclusion limits, it should be kept in mind that these are prone to the assumptions under which they were created.

Even when considering the largest uncertainties on the direct detection limits, the direct detection experiments are still able to test cross sections much smaller than the current LHC searches. This means that the overall picture of this summary plot does not change.

As [2] and [3] point out, more data is needed to gain more knowledge about the dark matter distribution in the Milky Way and the dark matter velocity distribution, but also about the visible matter components. For example, data from the GAIA telescope [70]

could give more information [2], while new insights at collider searches are expected for example from the upgraded LHC runs and the High-Luminosity LHC (HL-LHC) [14]. A plot summarising the expected limits from potential future collider and direct detection experiments can be found in appendix B.

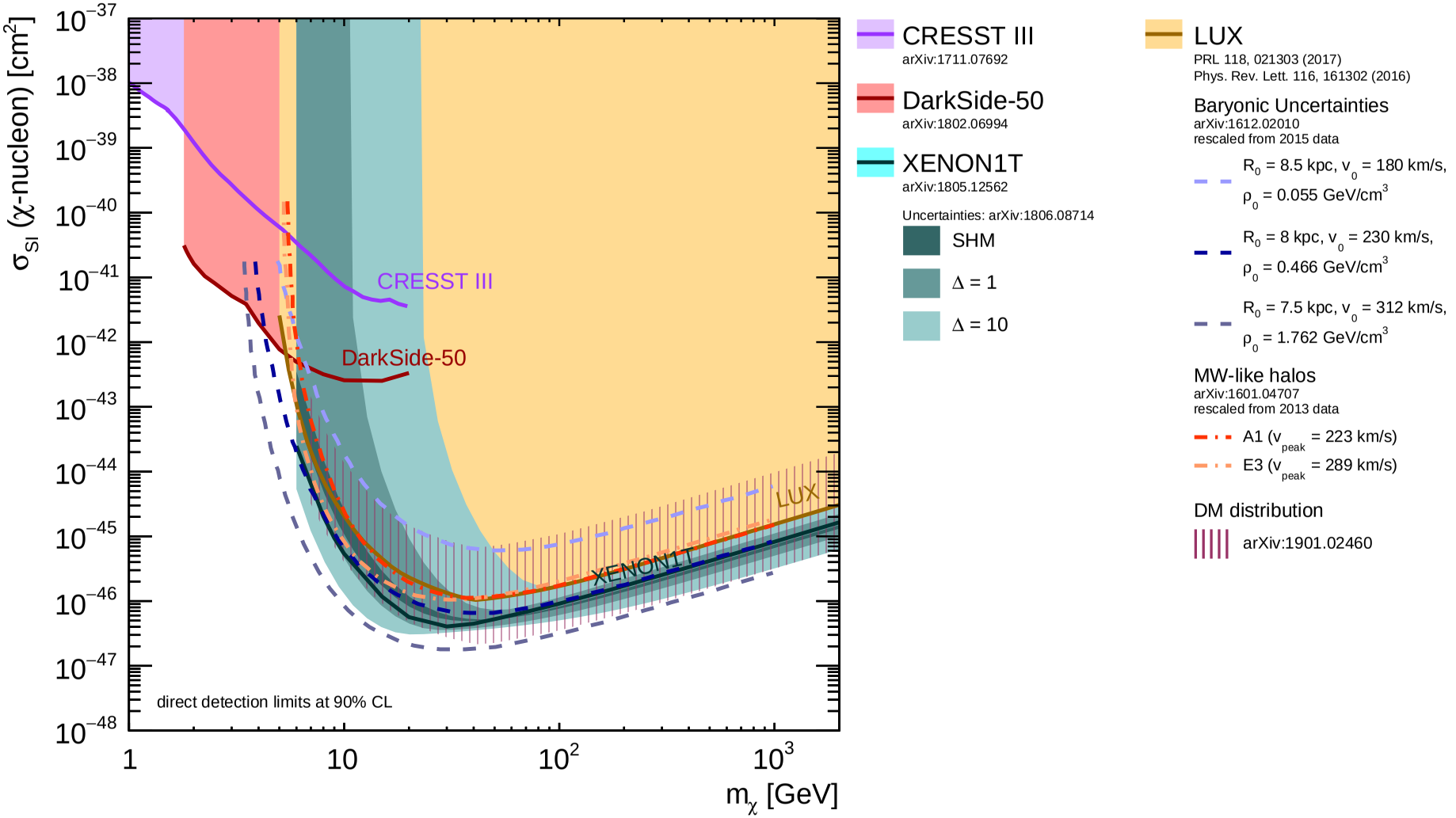

Figure 5.1: Exclusion plot with direct detection searches, including all deviations and uncertainty bands for direct detection limits.

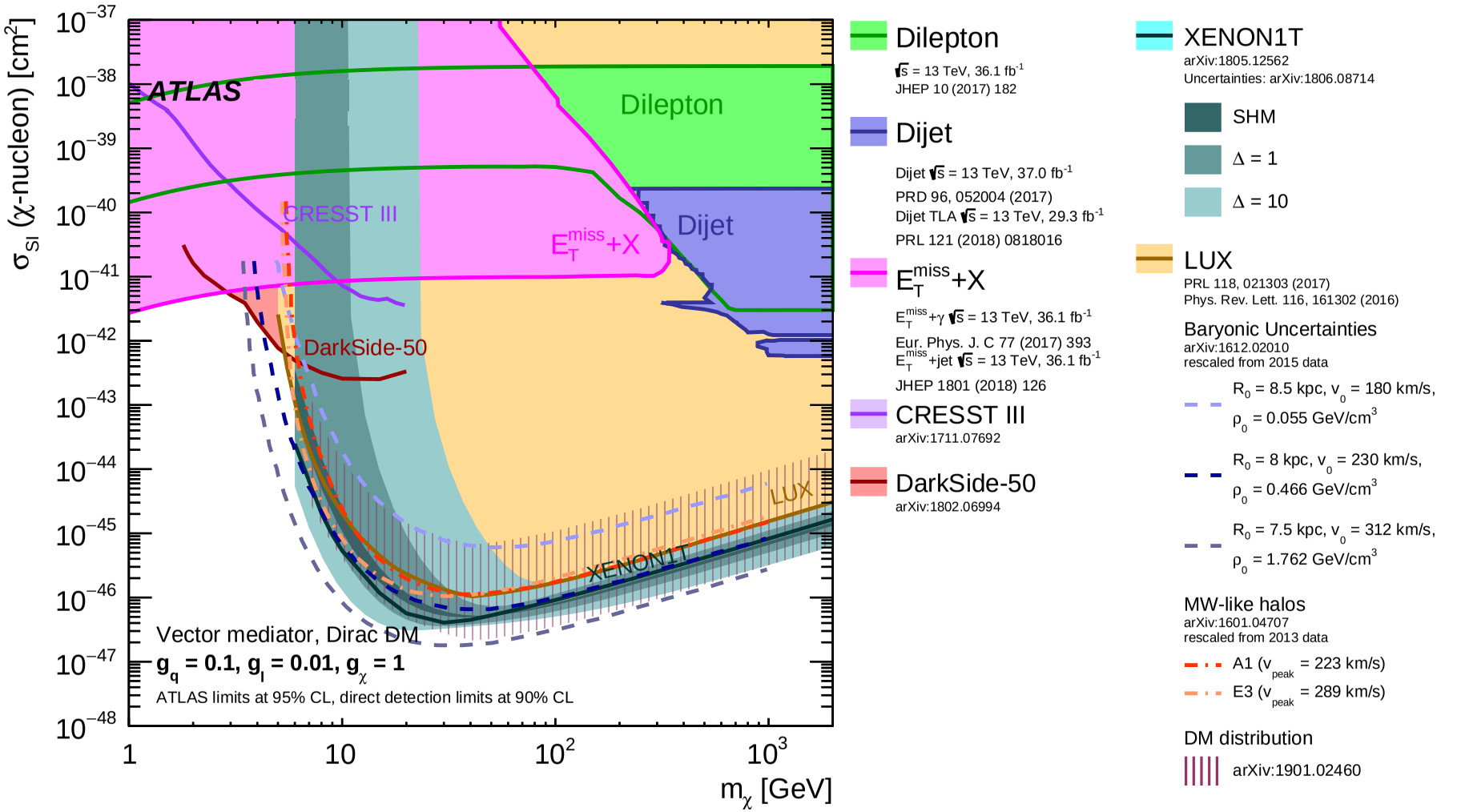

Figure 5.2: Exclusion plot with all LHC and direct detection searches, including deviations and uncertainty bands direct detection limits.

Chapter 6

Conclusions

The aim of this project was to combine astrophysical and particle physics approaches to constrain dark matter particle models, and to point out that to uncover the nature of dark matter, inputs from both astrophysics and particle physics are needed.

In the first part, it was shown that for a light vector mediator model, the current relic density value can be reproduced if the masses and couplings are chosen accordingly. In the standard thermal freeze-out scenario, for small mediator masses, the coupling to Standard Model particles has to be smaller compared to larger masses for the same dark matter coupling in order to not overproduce the relic density. This means that the lighter the mediator mass is, the more difficult it becomes to produce and measure this mediator at collider experiments, because the quark coupling constant needs to be small, which results in a small production rate in particle collisions. On the other hand, a lower centre-of-mass energy would be required to produce this light mediator. Furthermore, a change in the quark coupling has a larger impact on the relic density than a change in lepton couplings. For relic densities smaller than the current value, it is also possible to combine this WIMP dark matter model with other dark matter models that account for the remaining dark matter abundance, while the model is excluded for larger values.

These computations were done for two programmes, MadDM and micrOMEGAs, that give similar results, with only small deviations for light mediators, validating the programs.

In the second part, the relic density was investigated in freeze-in scenario in which the dark matter is produced over time from Standard Model particles that annihilate into the mediator. For this light mediator, the results indicate that in both off-shell and on-shell case the SM and DM coupling constants have to be extremely small to correctly reproduce the observed relic density. These couplings are too small to be currently detectable at the LHC.

In the third part, the dependence of the freeze-in relic density on the reheating temperature was tested. In the previous case, the reheating temperature was set to a high value, as often derived from theoretical predictions, but lower values are possible. For a quark coupling range that would be detectable at collider searches, it was found that the reheating temperature has to be in the order of a few GeV or less, as opposed to the previously assumed $3 \cdot 10^7$ GeV. This is a very broad range in possible values for the reheating temperature, which means that at the moment, for this model, a narrow estimate of the model parameters is not possible. More constraints from cosmology and astrophysics are needed to be able to bracket the particle dark matter models into a smaller parameter space.

In the fourth part, the astrophysical dependence of the results of direct detection experiments, aiming to detect the recoil of dark matter particles when scattering with target nuclei, was investigated. It was shown that the dark matter exclusion limits can shift by up to about an order of magnitude in cross section when assuming a different local dark matter density or velocity distribution. Uncertainties in the Galactic dark matter properties additionally arise from ignorance on the baryonic Milky Way components, such as the exact stellar content of the Galaxy. More precise data from astrophysical experiments could help to narrow down the uncertainties on these limits, giving a clearer picture of the exclusion area of the DM-nucleon scattering cross section, and thus on the

mass and couplings of the particle models. Additionally, there are uncertainties on the LHC searches that were not included in the summary plot in this work but should also be considered.

Chapter 7

Outlook

Since the discovery of dark matter, many efforts have been made to unveil its nature. While astrophysical observations have provided more information about dark matter, such as its fraction of the total content of the Universe, so that theories and models can be constrained accordingly, it has remained dark.

Many different types of experiments are built to search for evidence of particle dark matter. With telescopes becoming better to detect unusual signals in the Universe, direct detection experiments becoming bigger and more sensitive, and collider experiments reaching higher energies, more and more regions in the parameter space are tested for dark matter particles. Thus, if dark matter is indeed a particle phenomenon and if these particles interact with Standard Model particles, it should only be a question of time until dark matter can be discovered.

So far, no conclusive signal that indicates the existence of particle dark matter has been found. But when little is known about something, finding out what it is not is also valuable. This is implemented in exclusion plots that constrain the models and their parameter spaces, collecting data from many different types of searches, and taking the astrophysical and cosmological constraints into account. This can guide the design of experiments to search in regions of mass and interaction strength that have not been excluded or searched yet.

This work considered simple dark matter models and explored their constraints using astrophysical measurements of the dark matter relic density. Here, a caveat is that these models are based on simplified assumptions. The physics behind dark matter is likely more complicated than presented in the simplest models, but these simplified models can be made more complex when necessary. Furthermore, exclusion limits for these models from collider and direct detection searches were investigated. In this work, uncertainties were not added to the LHC searches, which is a possible future step. Deviations and uncertainty bands were implemented for some direct detection limits, as they depend on astrophysical properties, such as the local dark matter density and velocity, and the uncertainties in these affect the concluded exclusion limits for dark matter particle properties. Dark matter signals from the experiments could help to constrain these astrophysical parameters through the measured event rate.

In the next years, observations and measurements will be refined and taken to even higher energy scales and improved sensitivities, so that hopefully the mystery of dark matter will be solved, whatever its nature may be, bringing us another step forward to understanding the world.

Bibliography

[1] Alejandro Ibarra, Bradley J. Kavanagh, and Andreas Rappelt. "Bracketing the impact of astrophysical uncertainties on local dark matter searches". In: *JCAP* 1812.12 (2018), p. 018. DOI: 10.1088/1475-7516/2018/12/018. arXiv: 1806.08714 [hep-ph].

[2] Maria Benito et al. "Particle Dark Matter Constraints: the Effect of Galactic Uncertainties". In: *JCAP* 1702.02 (2017). [Erratum: JCAP1806,no.06,E01(2018)], p. 007. DOI: 10.1088/1475-7516/2017/02/007, 10.1088/1475-7516/2018/06/E01. arXiv: 1612.02010 [hep-ph].

[3] Nassim Bozorgnia et al. "Simulated Milky Way analogues: implications for dark matter direct searches". In: *JCAP* 1605.05 (2016), p. 024. DOI: 10.1088/1475-7516/2016/05/024. arXiv: 1601.04707 [astro-ph.CO].

[4] Maria Benito, Alessandro Cuoco, and Fabio Iocco. "Handling the Uncertainties in the Galactic Dark Matter Distribution for Particle Dark Matter Searches". In: *JCAP* 1903.03 (2019), p. 033. DOI: 10.1088/1475-7516/2019/03/033. arXiv: 1901.02460 [astro-ph.GA].

[5] *Code to create the ATLAS Dark Matter summary plots*. https://gitlab.cern.ch/atlas-phys-gen-common-dark-matter/tools/dmcombinationandinterpretation/tree/master.

[6] G. Bertone. *Particle Dark Matter: Observations, Models and Searches*. Cambridge University Press, 2010. ISBN: 9780521763684. URL: https://books.google.se/books?id=szrTSW07D-8C.

[7] Y. Akrami et al. *Planck 2018 results. I. Overview and the cosmological legacy of Planck*. 2018. arXiv: 1807.06205 [astro-ph.CO].

[8] Emma Ward. "Estimated matter-energy content of the Universe". General Photo. Mar. 2019. URL: https://cds.cern.ch/record/2665176.

[9] A. Liddle. *An Introduction to Modern Cosmology*. Wiley, 2015. ISBN: 9781118690253. URL: https://books.google.se/books?id=6n64CAAAQBAJ.

[10] G. Kane. *Modern Elementary Particle Physics: Explaining and Extending the Standard Model*. Cambridge University Press, 2017. ISBN: 9781107165083.

[11] B.R. Martin and G. Shaw. *Particle Physics*. 3rd edition. Wiley, 2009.

[12] *The Standard Model of Elementary Particles*. https://en.wikipedia.org/wiki/Standard_Model#/media/File:Standard_Model_of_Elementary_Particles.svg. Accessed 26-3-2019.

[13] C. Patrignani et al. "Review of Particle Physics". In: *Chin. Phys.* C40.10 (2016), p. 100001. DOI: 10.1088/1674-1137/40/10/100001.

[14] Antonio Boveia and Caterina Doglioni. "Dark Matter Searches at Colliders". In: *Ann. Rev. Nucl. Part. Sci.* 68 (2018), pp. 429–459. DOI: 10.1146/annurev-nucl-101917-021008. arXiv: 1810.12238 [hep-ex].

[15] Mauro Raggi, Venelin Kozhuharov, and P. Valente. *The PADME experiment at LNF*. 2015. arXiv: 1501.01867 [hep-ex].

[16] N. Aghanim et al. *Planck 2018 results. VI. Cosmological parameters*. 2018. arXiv: 1807.06209 [astro-ph.CO].

[17] K. N. Abazajian et al. *Light Sterile Neutrinos: A White Paper*. 2012. arXiv: 1204.5379 [hep-ph].

[18] Katelin Schutz et al. "Constraining a Thin Dark Matter Disk with Gaia". In: *Phys. Rev. Lett.* 121.8 (2018), p. 081101. DOI: 10.1103/PhysRevLett.121.081101. arXiv: 1711.03103 [astro-ph.GA].

[19] Marusa Bradac et al. "Strong and weak lensing united. 3. Measuring the mass distribution of the merging galaxy cluster 1E0657-56". In: *Astrophys. J.* 652 (2006), pp. 937–947. DOI: 10.1086/508601. arXiv: astro-ph/0608408 [astro-ph].

[20] C. Iliadis. *Nuclear Physics of Stars*. Physics Textbook. Wiley, 2015. ISBN: 9783527336487. URL: https://books.google.se/books?id=iUCkBgAAQBAJ.

[21] Timothy D. Brandt. "Constraints on MACHO Dark Matter from Compact Stellar Systems in Ultra-Faint Dwarf Galaxies". In: *Astrophys. J.* 824.2 (2016), p. L31. DOI: 10.3847/2041-8205/824/2/L31. arXiv: 1605.03665 [astro-ph.GA].

[22] Teresa Marrodán Undagoitia and Ludwig Rauch. "Dark matter direct-detection experiments". In: *J. Phys.* G43.1 (2016), p. 013001. DOI: 10.1088/0954-3899/43/1/013001. arXiv: 1509.08767 [physics.ins-det].

[23] P. Agnes et al. "Low-Mass Dark Matter Search with the DarkSide-50 Experiment". In: *Phys. Rev. Lett.* 121.8 (2018), p. 081307. DOI: 10.1103/PhysRevLett.121.081307. arXiv: 1802.06994 [astro-ph.HE].

[24] Caterina Doglioni and Antonio Boveia. *EFT Simplified Models*. https://commons.wikimedia.org/wiki/File:EFTSimplifiedModels.svg. Accessed: 2019-04-16.

[25] *The MAGIC Telescopes*. https://magic.mpp.mpg.de/. Accessed: 2019-04-22.

[26] *H.E.S.S.* https://www.mpi-hd.mpg.de/hfm/HESS/. Accessed: 2019-04-22.

[27] *The IceCube Neutrino Observatory*. https://icecube.wisc.edu/. Accessed: 2019-04-22.

[28] *Super-Kamiokande*. http://www-sk.icrr.u-tokyo.ac.jp/sk/index-e.html. Accessed: 2019-04-22.

[29] M. Casolino and The Pamela collaboration. "The Pamela Cosmic Ray Space Observatory: Detector, Objectives and First Results". In: *arXiv e-prints*, arXiv:0904.4692 (Apr. 2009), arXiv:0904.4692. arXiv: 0904.4692 [astro-ph.HE].

[30] *XENON1T Experiment*. http://www.xenon1t.org/. Accessed: 2019-02-12.

[31] *LUX Dark Matter Experiment*. http://luxdarkmatter.org/. Accessed: 2019-04-06.

[32] D. S. Akerib et al. "Results from a search for dark matter in the complete LUX exposure". In: *Phys. Rev. Lett.* 118.2 (2017), p. 021303. DOI: 10.1103/PhysRevLett.118.021303. arXiv: 1608.07648 [astro-ph.CO].

[33] D. S. Akerib et al. "Results on the Spin-Dependent Scattering of Weakly Interacting Massive Particles on Nucleons from the Run 3 Data of the LUX Experiment". In: *Phys. Rev. Lett.* 116.16 (2016), p. 161302. DOI: 10.1103/PhysRevLett.116.161302. arXiv: 1602.03489 [hep-ex].

[34] *CRESST*. https://www.cresst.de/. Accessed: 2019-04-22.

[35] *PandaX*. https://pandax.sjtu.edu.cn/. Accessed: 2019-04-22.

[36] *The Large Hadron Collider*. https://home.cern/science/accelerators/large-hadron-collider. Accessed: 2019-04-3.

[37] Daniel Abercrombie et al. "Dark Matter Benchmark Models for Early LHC Run-2 Searches: Report of the ATLAS/CMS Dark Matter Forum". In: (2015). Ed. by Antonio Boveia et al. arXiv: 1507.00966 [hep-ex].

[38] Andreas Albert et al. *Recommendations of the LHC Dark Matter Working Group: Comparing LHC searches for heavy mediators of dark matter production in visible and invisible decay channels*. 2017. arXiv: 1703.05703 [hep-ex].

[39] Emma Ward. "Key Particle Discoveries Timeline". General Photo. Mar. 2019. URL: https://cds.cern.ch/record/2665175.

[40] Mihailo Backovic, Kyoungchul Kong, and Mathew McCaskey. *MadDM v.1.0: Computation of Dark Matter Relic Abundance Using MadGraph5*. 2014. arXiv: 1308.4955 [hep-ph].

[41] G. Bélanger et al. *The user's manual, version 4.3*. https://lapth.cnrs.fr/micromegas/v4.3/manual4.3.pdf. Accessed: 2018-05-31.

[42] J. Alwall et al. "The automated computation of tree-level and next-to-leading order differential cross sections, and their matching to parton shower simulations". In: *JHEP* 07 (2014), p. 079. DOI: 10.1007/JHEP07(2014)079. arXiv: 1405.0301 [hep-ph].

[43] Caterina Doglioni and Antonio Boveia. *MonoX*. https://commons.wikimedia.org/wiki/File:MonoX.svg. Accessed: 2019-04-16.

[44] G. Barr et al. *Particle Physics in the LHC Era*. Oxford Master Series in Physics. OUP Oxford, 2016. ISBN: 9780191065453. URL: https://books.google.se/books?id=LrgoCwAAQBAJ.

[45] Giorgio Busoni et al. *Recommendations on presenting LHC searches for missing transverse energy signals using simplified s-channel models of dark matter*. Ed. by Antonio Boveia et al. 2016. arXiv: 1603.04156 [hep-ex].

[46] James S. Bullock and Michael Boylan-Kolchin. "Small-Scale Challenges to the ΛCDM Paradigm". In: *Ann. Rev. Astron. Astrophys.* 55 (2017), pp. 343–387. DOI: 10.1146/annurev-astro-091916-055313. arXiv: 1707.04256 [astro-ph.CO].

[47] Nicolás Bernal et al. "The Dawn of FIMP Dark Matter: A Review of Models and Constraints". In: *Int. J. Mod. Phys.* A32.27 (2017), p. 1730023. DOI: 10.1142/S0217751X1730023X. arXiv: 1706.07442 [hep-ph].

[48] Lawrence J. Hall et al. *Freeze-In Production of FIMP Dark Matter*. 2010. arXiv: 0911.1120 [hep-ph].

[49] Geneviève Bélanger et al. "micrOMEGAs5.0: Freeze-in". In: *Comput. Phys. Commun.* 231 (2018), pp. 173–186. DOI: 10.1016/j.cpc.2018.04.027. arXiv: 1801.03509 [hep-ph].

[50] Steen Hannestad. "What is the lowest possible reheating temperature?" In: *Phys. Rev.* D70 (2004), p. 043506. DOI: 10.1103/PhysRevD.70.043506. arXiv: astro-ph/0403291 [astro-ph].

[51] A. M. Sirunyan et al. "Search for new physics in final states with an energetic jet or a hadronically decaying W or Z boson and transverse momentum imbalance at $\sqrt{s} = 13$ TeV". In: *Phys. Rev.* D97.9 (2018), p. 092005. DOI: 10.1103/PhysRevD.97.092005. arXiv: 1712.02345 [hep-ex].

[52] *ROOT*. https://root.cern.ch/. Accessed: 2018-09-12.

[53] private communication.

[54] E. Aprile et al. "Dark Matter Search Results from a One Ton-Year Exposure of XENON1T". In: *Phys. Rev. Lett.* 121.11 (2018), p. 111302. DOI: 10.1103/PhysRevLett.121.111302. arXiv: 1805.12562 [astro-ph.CO].

[55] *The XENON Dark Matter Project*. http://xenon.astro.columbia.edu/XENON10_Experiment/. Accessed: 2019-05-02.

[56] E. Aprile et al. "Intrinsic backgrounds from Rn and Kr in the XENON100 experiment". In: *Eur. Phys. J.* C78.2 (2018), p. 132. DOI: 10.1140/epjc/s10052-018-5565-y. arXiv: 1708.03617 [astro-ph.IM].

[57] Morad Aaboud et al. "Constraints on mediator-based dark matter and scalar dark energy models using $\sqrt{s} = 13$ TeV pp collision data collected by the ATLAS detector". In: (2019). arXiv: 1903.01400 [hep-ex].

[58] *Summary plots from the ATLAS Exotic physics group*. https://atlas.web.cern.ch/Atlas/GROUPS/PHYSICS/CombinedSummaryPlots/EXOTICS/. Accessed: 2019-04-20.

[59] Morad Aaboud et al. "Search for new high-mass phenomena in the dilepton final state using 36 fb^{-1} of proton-proton collision data at $\sqrt{s} = 13$ TeV with the ATLAS detector". In: *JHEP* 10 (2017), p. 182. DOI: 10.1007/JHEP10(2017)182. arXiv: 1707.02424 [hep-ex].

[60] Morad Aaboud et al. "Search for new phenomena in dijet events using 37 fb^{-1} of pp collision data collected at $\sqrt{s}$ =13 TeV with the ATLAS detector". In: *Phys. Rev.* D96.5 (2017), p. 052004. DOI: 10.1103/PhysRevD.96.052004. arXiv: 1703.09127 [hep-ex].

[61] M. Aaboud et al. "Search for low-mass dijet resonances using trigger-level jets with the ATLAS detector in pp collisions at $\sqrt{s} = 13$ TeV". In: *Phys. Rev. Lett.* 121.8 (2018), p. 081801. DOI: 10.1103/PhysRevLett.121.081801. arXiv: 1804.03496 [hep-ex].

[62] Morad Aaboud et al. "Search for dark matter at $\sqrt{s} = 13$ TeV in final states containing an energetic photon and large missing transverse momentum with the ATLAS detector". In: *Eur. Phys. J.* C77.6 (2017), p. 393. DOI: 10.1140/epjc/s10052-017-4965-8. arXiv: 1704.03848 [hep-ex].

[63] Morad Aaboud et al. "Search for dark matter and other new phenomena in events with an energetic jet and large missing transverse momentum using the ATLAS detector". In: *JHEP* 01 (2018), p. 126. DOI: 10.1007/JHEP01(2018)126. arXiv: 1711.03301 [hep-ex].

[64] *ATLAS Experiment at CERN*. http://atlas.cern/. Accessed: 2019-04-25.

[65] Ronald L. Wasserstein and Nicole A. Lazar. "The ASA's Statement on p-Values: Context, Process, and Purpose". In: *The American Statistician* 70.2 (2016), pp. 129–133. DOI: 10.1080/00031305.2016.1154108. eprint: https://doi.org/10.1080/00031305.2016.1154108. URL: https://doi.org/10.1080/00031305.2016.1154108.

[66] Matthieu Schaller et al. "The EAGLE simulations of galaxy formation: the importance of the hydrodynamics scheme". In: *Mon. Not. Roy. Astron. Soc.* 454.3 (2015), pp. 2277–2291. DOI: 10.1093/mnras/stv2169. arXiv: 1509.05056 [astro-ph.GA].

[67] private communication, to be published.

[68] *Script to calculate uncertainty bands for direct detection exclusion limits*. https://github.com/IsabelleJohn/DDuncertainties.

[69] Alis J. Deason et al. "The local high-velocity tail and the Galactic escape speed". In: *Monthly Notices of the Royal Astronomical Society* 485.3 (May 2019), pp. 3514–3526. DOI: 10.1093/mnras/stz623. arXiv: 1901.02016 [astro-ph.GA].

[70] Gaia Collaboration. "The Gaia mission". In: *Astronomy & Astrophysics* 595, A1 (Nov. 2016), A1. DOI: 10.1051/0004-6361/201629272. arXiv: 1609.04153 [astro-ph.IM].

[71] Spain. 2019. Granada. *European Strategy for Particle Physics*. https://cafpe.ugr.es/eppsu2019/.

[72] *European Strategy for Particle Physics*. https://europeanstrategy.cern/.

[73] Philip Harris et al. "Closing up on dark sectors at colliders: From 14 to 100 TeV". In: *Phys. Rev. D* 93 (5 Mar. 2016), p. 054030. DOI: 10.1103/PhysRevD.93.054030. URL: https://link.aps.org/doi/10.1103/PhysRevD.93.054030.

[74] Xabier Cid Vidal et al. "Beyond the Standard Model Physics at the HL-LHC and HE-LHC". In: (2018). arXiv: 1812.07831 [hep-ph].

[75] J. Aalbers et al. "DARWIN: towards the ultimate dark matter detector". In: *JCAP* 1611 (2016), p. 017. DOI: 10.1088/1475-7516/2016/11/017. arXiv: 1606.07001 [astro-ph.IM].

[76] Caterina Doglioni. *Dark Matter at Colliders*. European Strategy for Particle Physics, Grenada, May 2019, https://indico.cern.ch/event/808335/contributions/3373983/attachments/1843062/3023210/20180513_Doglioni_DM_EPPSU.pdf.

[77] To appear in European Strategy briefing book.

Appendices

Appendix A

Computation of uncertainty bands

This section describes how the LUX limits can be reinterpreted when looking at different values for the Standard Galactic parameters. The method of handling the Galactic uncertainties comes from this paper [4], and instructions are given in [67]. The code performing these calculations can be found in [68].

For a direct detection experiment, the differential event rate is

$$\frac{\mathrm{d}R}{\mathrm{d}E_R} = \rho_0 C_{\mathrm{PP}}\, \eta\left(v_{\min}, t\right) \tag{A.1}$$

where C_{PP} contains all input with particle or nuclear physics dependence. The local dark matter density, ρ_0, and the halo integral, η, are astrophysical inputs that are subjected to astrophysical uncertainties.

The halo integral is given by

$$\eta\left(v_{\min}, t\right) \equiv \int_{v_{\min}}^{v_{\mathrm{esc}}} \mathrm{d}^3 v\, \frac{f_{\mathrm{det}}\left(\vec{v}, t\right)}{v}, \tag{A.2}$$

where in this case the escape velocity of the Galaxy, v_{esc}, the minimum velocity a particle has to have to leave the gravitational potential of the Milky Way, is assumed to be the maximum velocity of the dark matter particles, supposing that faster particles would have escaped the Galaxy. Then $v_{\min}$ is the minimum velocity an incoming dark matter particle has to have in order to deposit a recoil energy E_R that the detector is sensitive to. This is calculated by

$$v_{\min} = \sqrt{\frac{m_A E_R}{2\mu_A^2}}. \tag{A.3}$$

For LUX, the minimum recoil energy measurable by the detector is $E_R = 1.1 \cdot 10^{-6}$ GeV, taken from [32, 33]. As the target material is xenon, $m_A = 122$ GeV/c^2, and the reduced mass depends on the dark matter particle mass, $\mu_A = m_{\mathrm{DM}} m_A/(m_{\mathrm{DM}} + m_A)$.

The halo integral also includes the velocity distribution of the dark matter particles. In this case, the velocity distribution is assumed to follow a Maxwell-Boltzmann distribution,

$$f_{\mathrm{MB}}\left(\vec{v}\right) = \frac{1}{\left(\pi v_0^2\right)^{3/2} N_{\mathrm{esc}}} \exp\left(-\frac{\left(\vec{v} + \vec{v}_{\oplus}\left(t\right)\right)^2}{v_0^2}\right), \tag{A.4}$$

truncated at the Galactic escape speed, where f_{MB} is normalised to 1, and the normalisation constant N_{esc} is

$$N_{\mathrm{esc}} = \mathrm{erf}\left(\frac{v_{\mathrm{esc}}}{v_0}\right) - \frac{2}{\sqrt{\pi}} \frac{v_{\mathrm{esc}}}{v_0} \exp\left(-\left(\frac{v_{\mathrm{esc}}}{v_0}\right)^2\right). \tag{A.5}$$

According to chapter 17.3.3 in [6], the velocity of Earth's orbit can be approximated by just the circular velocity of the Sun, $\vec{v}_0 = (0, 220, 0)$ km/s. This drops the time-dependence of the halo integral. To perform the integral, spherical coordinates are introduced. Equation A.2 then becomes

$$\eta\left(v_{\min}\right)=\int_{v_{\min}}^{v_{\mathrm{esc}}}\int_{0}^{2\pi}\int_{0}^{\pi}\frac{1}{\left(\pi v_{0}^{2}\right)^{3/2}N_{\mathrm{esc}}}\times$$
$$\exp\left(-\frac{\left(v\sin\theta\cos\varphi+v_{0}^{x}\right)^{2}+\left(v\sin\theta\sin\varphi+v_{0}^{y}\right)^{2}+\left(v\cos\theta+v_{0}^{z}\right)^{2}}{v_{0}^{2}}\right)v\sin\theta\,\mathrm{d}\theta\,\mathrm{d}\varphi\,\mathrm{d}v. \tag{A.6}$$

The analysis group provides a likelihood profile for the grid $(v_0, \rho_0, v_{\mathrm{esc}})$ with corresponding χ^2 fit. Each grid point gives a different combination of the values v_0, ρ_0 and v_{esc}, thus each providing a different uncertainty from Galactic parameters. To reduce computing time, it is enough to only use the grid points with $\chi^2 < 50$ and a number of bins for the χ^2 profile of 38.

The experimental limits are given in the parameter space $(m_{\mathrm{DM}}, \sigma)$. In this method, for each m_{DM}, the corresponding cross section is multiplied by a factor to obtain the new limit.

According to the instruction, in the first step, the limit given by the experiment is updated. First, from the given likelihood profile, the grid point with the smallest χ^2 (i.e. the best fit, as a χ^2 value close to 1 indicates), is selected. This factor is called $(\rho_0 \times \eta(v_{\min}))_{\mathrm{BF}}$.

Additionally, the factor $\rho_0 \times \eta$ is calculated with the assumptions made by the experiment. In the case of LUX, this follows the Standard Halo Model (SHM), with $\rho_0 = 0.3$ GeV/cm^3, $v_0 = 220$ km/s, $v_{\mathrm{esc}} = 544$ km/s, and a Maxwell-Boltzmann velocity distribution similarly. For each m_{DM}, the corresponding cross section is thus multiplied by the ratio

$$\frac{\left(\rho_0 \times \eta\left(v_{\min}\right)\right)_{\mathrm{BF}}}{\rho_0^{\mathrm{exp}} \times \eta^{\mathrm{exp}}\left(v_{\min}\right)}. \tag{A.7}$$

In the next step, for all grid points in the likelihood profile, the χ^2 profile is calculated for the factor $\rho_0 \times \eta$. Then, a subset is selected, fulfilling the condition

$$\chi^2 \leq \chi^2_{\mathrm{BF}} + \chi^2_{2\sigma}(1) \tag{A.8}$$

with $\chi^2_{2\sigma}(1) = 4$ being the χ^2 for 2σ. χ^2_{BF} is the minimum χ^2 from all grid points, as selected in the first step. χ^2 is the χ^2 corresponding to each grid point.

From this subset, the minimum and maximum factor $\rho_0 \times \eta$ are selected, leading to two factors, one giving the upper limit of the uncertainty band, the other one the lower limit, that are multiplied by the updated cross section from the previous step:

$$\frac{\left(\rho_0 \times \eta\left(v_{\min}\right)\right)_{\min}}{\left(\rho_0 \times \eta\left(v_{\min}\right)\right)_{\mathrm{BF}}} \quad \text{and} \quad \frac{\left(\rho_0 \times \eta\left(v_{\min}\right)\right)_{\max}}{\left(\rho_0 \times \eta\left(v_{\min}\right)\right)_{\mathrm{BF}}}. \tag{A.9}$$

In principle, the factor $\left(\rho_0 \times \eta\left(v_{\min}\right)_{\mathrm{BF}}\right.$ should be the same in both steps.

Repeating this for all m_{DM} and corresponding cross section, an uncertainty band for the experimental limit is obtained.

Appendix B

Future collider and direct detection experiments

Figure B.1 was created in the context of the European Strategy for Particle Physics [71, 72], a process to discuss and determine the direction of particle physics and potential future particle physics experiments.

The plot summarises exclusion limits from collider and direct detection experiments, similar to the previously shown plots (see e.g. figure 5.2), here for a scalar mediator [37]. It also contains the expected exclusion limits from potential future collider experiments, such as the Future Circular Collider (FCC) [73] and the High Luminosity and High Energy LHC (HL-LHC and HE-LHC) [74], and potential direct detection experiments, such as DARWIN-200 [75]. These experiments could probe cross sections smaller by several orders of magnitude than current experiments, and would thus greatly expand the search for particle dark matter. For a dark matter mass region from about 400 GeV to about 1000 GeV, future collider and direct detection search strategies cover a similar parameter space and are thus complementary. To detect and identify dark matter particles, these complementary searches are needed, as collider experiments can produce invisible particles and determine the properties of the mediator, while direct detection experiments are needed to validate that the particle is indeed a dark matter particle (see chapter 4).

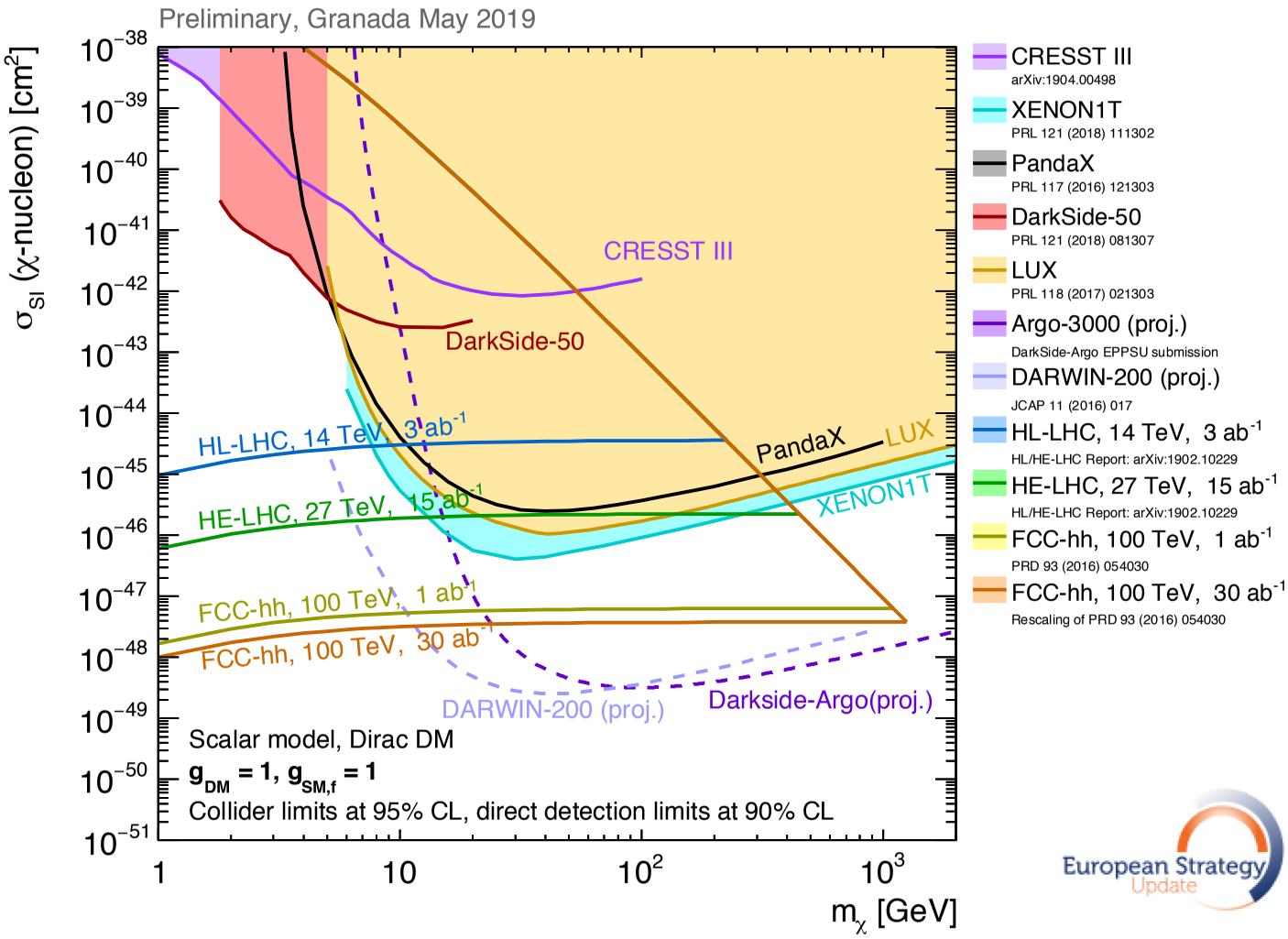

Figure B.1: Summary plot presenting the current limits of direct detection experiments as shown previously, and expected limits from potential future collider and direct detection experiments, indicating that the complementary of the different dark matter searches continues. Here, the mediator model is a scalar mediator. Figure from [76, 77].